Article:
Witkos, Tomasz M., Chan, Wing Lee, Joensuu, Merja et al. (14 more authors) (2019) GORAB scaffolds COPI at the trans-Golgi for efficient enzyme recycling and correct protein glycosylation. Nature Communications. 127. ISSN 2041-1723

https://doi.org/10.1038/s41467-018-08044-6

GORAB scaffolds COPI at the *trans*-Golgi for efficient enzyme recycling and correct protein glycosylation

Tomasz M. Witkos[1], Wing Lee Chan[2,3], Merja Joensuu[4,5], Manuel Rhiel[6], Ed Pallister[8], Jane Thomas-Oates[8], A. Paul Mould[1], Alex A. Mironov[1], Christophe Biot[9], Yann Guerardel[9], Willy Morelle[9], Daniel Ungar[7], Felix T. Wieland[6], Eija Jokitalo[4], May Tassabehji[1,10], Uwe Kornak[2,3] and Martin Lowe[1,11]

[1] School of Biology, Faculty of Biology, Medicine and Health, University of Manchester, The Michael Smith Building, Oxford Road, Manchester, UK.

[2] Berlin-Brandenburg Centre for Regenerative Therapies (BCRT), Institut fuer Medizinische Genetik und Humangenetik, Charité – Universitätsmedizin Berlin, corporate member of Freie Universität Berlin, Humboldt-Universität zu Berlin, and Berlin Institute of Health, Berlin, Germany.

[3] FG Development & Disease, Max Planck Institut fuer Molekulare Genetik, Berlin, Germany.

[4] Cell and Molecular Biology Program, Institute of Biotechnology, University of Helsinki, Helsinki, Finland

[5]Present address: Clem Jones Centre of Ageing Dementia Research, Queensland Brain Institute, The University of Queensland, Brisbane, Australia, and Minerva Foundation Institute for Medical Research, 00290 Helsinki, Finland

[6] Heidelberg University Biochemistry Center, Heidelberg University, Heidelberg, Germany.

[7]Department of Biology, University of York, York, UK.

[8] Department of Chemistry, University of York, York, UK.

[9]Univ. Lille, CNRS, UMR 8576 - UGSF - Unité de Glycobiologie Structurale et Fonctionnelle, F-59000 Lille, France.

[10]Manchester Centre for Genomic Medicine, St. Mary's Hospital, Manchester Academic Health Sciences Centre (MAHSC), Manchester, UK.

[11]To whom correspondence should be addressed: Tel: 0161-275-5387. Fax: 0161-275-1505. E-mail: martin.lowe@manchester.ac.uk

Abstract

COPI is a key mediator of protein trafficking within the secretory pathway. COPI is recruited to the membrane primarily through binding to Arf GTPases, upon which it undergoes assembly to form coated transport intermediates responsible for trafficking numerous proteins, including Golgi-resident enzymes. Here, we identify GORAB, the protein mutated in the skin and bone disorder gerodermia osteodysplastica, as a component of the COPI machinery. GORAB forms stable domains at the *trans*-Golgi that, via interactions with the COPI-binding protein Scyl1, promote COPI recruitment to these domains. Pathogenic GORAB mutations perturb Scyl1 binding or GORAB assembly into domains, indicating the importance of these interactions. Loss of GORAB causes impairment of COPI-mediated retrieval of *trans*-Golgi enzymes, resulting in a deficit in glycosylation of secretory cargo proteins. Our results therefore identify GORAB as a COPI scaffolding factor, and support the view that defective protein glycosylation is major disease mechanism in gerodermia osteodysplastica.

52 **Introduction**

53 COPI-coated transport vesicles mediate protein trafficking in the early secretory
54 pathway. They are responsible for retrograde transport from the Golgi apparatus
55 to the endoplasmic reticulum (ER) [1], and for trafficking between cisternae within
56 the Golgi apparatus [2-4]. Within the Golgi, COPI-coated vesicles mediate
57 retrograde traffic of Golgi resident enzymes [5,6], and may also participate in
58 anterograde trafficking of certain cargoes [7,8]. Although COPI is best known for its
59 role in vesicle trafficking, recent studies also suggest possible involvement in
60 trafficking via tubular intermediates at the level of the Golgi stack [9]. In line with
61 its trafficking functions, COPI is localized at the ER-to-Golgi intermediate
62 compartment (ERGIC) and Golgi apparatus, where it is abundant at the cisternal
63 rims and enriched towards the *cis*-side [10,11]. The COPI coat is comprised of the
64 hetero-heptameric coatomer complex [2], which is recruited from the cytosol to
65 the membrane by the small GTPase Arf1 [12,13], which itself is recruited from the
66 cytosol concomitant with GTP loading [14]. Coatomer functions to both select cargo
67 and promote vesicle formation [15,16], which is facilitated by the assembly of
68 coatomer complexes into a cage-like structure [17,18]. Although Arf1 is the primary
69 driver of coatomer recruitment, additional factors may contribute to this
70 process. The p24 family proteins have been proposed to function as coatomer
71 receptors [15,19], but the extent to which other proteins participate in coatomer
72 recruitment or assembly is poorly understood.

73 The cutis laxa syndromes are defined by the presence of loose, wrinkly,
74 inelastic skin and can be classified into various types depending upon clinical
75 features and the gene that is mutated [20]. The skin phenotype seen in cutis laxa is

76 thought to arise from defective production and/or assembly of extracellular
77 matrix, predominantly at the level of elastic fibres [21]. Mutations in several elastic
78 fibre proteins have been shown to cause cutis laxa, but interestingly, causative
79 mutations in several cellular proteins have also been identified [20,21]. Amongst
80 these is GORAB, also known as Scyl1BP1, whose mutation is responsible for
81 gerodermia osteodysplastica (GO) [22]. The hallmark symptoms of GO are cutis
82 laxa and osteoporosis, with reduced bone mass and susceptibility to fractures
83 [23,24]. As both symptoms are features of aging, GO as been classified as a progeroid
84 disorder [22]. Hence, understanding how loss of GORAB leads to pathological
85 changes in skin and bone is likely to give new insight into how these tissues age.

86 GORAB is localized to the *trans*-side of the Golgi apparatus [22]. It is
87 comprised of a central coiled-coil region that is responsible for Golgi targeting,
88 most likely via interactions with the small GTPases Rab6 and Arf5 [25]. It has been
89 proposed that GORAB is a member of the golgin family of coiled-coil Golgi
90 proteins [22], which participate in vesicle tethering [26,27]. GORAB has also been
91 proposed to function as a transcriptional activator for neurite outgrowth [28], as a
92 modulator of MDM2 ubiquitylation that in turn can impact upon p53 levels and
93 apoptosis [29], and has recently been shown to play a role in centriole duplication
94 and ciliogenesis [30,31]. Despite these advances, the function of Golgi-associated
95 GORAB remains poorly defined, and the pathogenic mechanism underlying GO
96 remains to be determined. Here, we show that GORAB functions in intra-Golgi
97 trafficking as a scaffolding protein for COPI. It forms stable membrane domains
98 that, via interaction with Scyl1, stabilize COPI assembly at the *trans*-Golgi. Loss of
99 GORAB function results in reduced recycling of *trans*-Golgi enzymes and

100 improper glycosylation of cargo proteins within both cultured cells and skin
101 tissue. Our results therefore identify GORAB as a player in COPI trafficking, and
102 provide a mechanism to explain the symptoms of GO that are also relevant to
103 human ageing.

104

105 **Results**

106 **GORAB interacts with Scyl1**

107 To gain insight into the cellular functions of GORAB we first investigated its
108 interaction partners. GORAB was first identified as a potential binding partner
109 for Scyl1 [32], also known as NTKL, but this interaction has yet to be validated. We
110 therefore determined whether Scyl1 is a bona fide interactor of GORAB. GORAB
111 bound to Scyl1 in the yeast two-hybrid system (Fig 1A). GORAB and Scyl1 self-
112 association was also detected in the yeast two-hybrid system, consistent with the
113 presence of coiled-coil and HEAT repeat domains respectively in these proteins
114 (see Fig 1D and E) [33]. GORAB and Scyl1 interaction was confirmed in protein
115 pull-down experiments (Fig 1B). The binding between GORAB and Scyl1 is
116 direct, as indicated by pull-down experiments with purified recombinant
117 proteins (Fig 1C). We next mapped the interaction sites in GORAB and Scyl1.
118 GORAB is comprised of a central coiled-coil region, with several predicted breaks
119 within the coiled-coil (Fig 1D, right), flanked by non-coiled N- and C-terminal
120 domains. Pull-down experiments with purified proteins indicated that the N-
121 terminal non-coil domain is sufficient to bind Scyl1 (Fig 1D, left). Scyl1 is
122 comprised of an N-terminal kinase-like domain that is predicted to be
123 catalytically inactive, centrally-located HEAT repeats and a C-terminal short
124 coiled-coil domain followed by a dibasic binding motif for the coatomer complex
125 of the COPI vesicle coat [34] (Fig 1E, right). Mapping experiments indicated that the
126 binding site for GORAB resides within the kinase-like domain of Scyl1 (Fig 1E,
127 left). Thus, GORAB and Scyl1 are bona fide binding partners that directly interact
128 via their respective N-terminal domains.

129

130 **GORAB forms discrete domains at the *trans*-Golgi**

131 GORAB was previously localized to the *trans*-Golgi by immunofluorescence
132 microscopy [22,25]. We were therefore unsurprised to find extensive co-localization
133 of GORAB with the *trans*-Golgi marker TGN46 by immunofluorescence
134 microscopy (Fig 2A). However, interestingly, closer inspection revealed that,
135 unlike TGN46, GORAB was not evenly distributed throughout the *trans*-Golgi but
136 rather concentrated in discrete puncta (Fig 2A). The puncta disappeared upon
137 depletion of GORAB, and were also observed with over-expressed GFP-tagged
138 GORAB, confirming specificity of the staining (Fig 2B). The discrete nature of the
139 GORAB puncta was further revealed by super-resolution (Fig 2C) and immuno-
140 electron microscopy of both HeLa cells and dermal fibroblasts (Fig 2D and E).
141 The GORAB puncta are enriched at the *trans*-side of the Golgi and found
142 predominantly within the tubulo-vesicular *trans*-Golgi network, as well as
143 occasionally at the rims of the *trans*-most Golgi cisternae (Fig 2D and E).

144 Previous work has shown that Scyl1 distribution is biased towards the
145 *cis*-Golgi, with a significant pool in the ER-Golgi intermediate compartment
146 ERGIC) [34]. Labeling for Scyl1 indicated its presence in numerous puncta within
147 the Golgi region and in more peripheral ERGIC (Supplementary Figure 1A). As
148 expected, many of the Golgi puncta overlap with the *cis*-Golgi marker GM130,
149 however there was also significant overlap of Scyl1 puncta with TGN46,
150 indicating that a pool of Scyl1 also resides at the *trans*-Golgi (Supplementary
151 Figure 1A). In agreement, we observed colocalization of Scyl1 puncta with
152 GORAB (Supplementary Figure 1B, see also Fig 2F). Although GORAB cannot

153 bind directly to COPI (Supplementary Figure 1C), Scyl1 does, via its extreme C-
154 terminus (Supplementary Figures 1C and 1D)[34], which interacts with the γ-COP
155 appendage domain (Supplementary Figure 1E)[33], and a second site within the β'-
156 COP subunit [35]. We therefore investigated whether the GORAB and Scyl1 puncta
157 also contained COPI. As shown in Fig 2F, using super resolution microscopy we
158 could show that many of the GORAB and Scyl1 positive puncta are also positive
159 for COPI. Interestingly, Scyl1 frequently appeared to localize between GORAB
160 and COPI, consistent with it bridging these two factors (Fig 2F). We never
161 observed COPI in the GORAB puncta in the absence of Scyl1, whereas the
162 opposite could occur, consistent with the view that Scyl1 is required for COPI
163 association with the GORAB puncta (Fig 2F). We could also detect overlap of
164 Rab6 with the GORAB puncta, as expected from the known interaction of GORAB
165 with Rab6 [22], although Rab6 was also present outside these regions, consistent
166 with it interacting with various effector proteins involved in different processes
167 at the Golgi (Fig 2G) [36].

168

169 **GORAB and Scyl1 are Arf effector proteins**

170 A recent study described binding of GORAB to Arf5, a Golgi-localized class II Arf
171 [25]. Given the association of GORAB, via Scyl1, with COPI, and the fact that class I
172 and II Arf GTPases both promote membrane recruitment of COPI [37], we re-
173 evaluated GORAB interaction with Arfs. Using pull-downs, we could show that
174 GORAB is able to bind to the class I Arfs, Arf1 and Arf3, in addition to Arf5
175 (Supplementary Figure 1F). Binding occurred only to the active, GTP-bound form
176 and appeared strongest to class I Arfs. We also investigated Scyl1 binding to Arfs.

177 It has been reported that Scyl1 binds selectively to class II Arfs, and that binding
178 is independent of nucleotide status [33]. We observed binding of Scyl1 to Arfs, but
179 binding was to class I Arfs only, with strongest binding to Arf1, and binding was
180 only to the active GTP-bound form (Supplementary Figure 1F). Binding of both
181 GORAB and Scyl1 to Arf1 is direct (Supplementary Figure 1G). These results
182 suggest that GORAB and Scyl1 function as Arf effector proteins. Interactions
183 between GORAB, Scyl1, COPI and Arf1 were not mutually exclusive, as indicated
184 by pull-down experiments, consistent with the proteins functioning together in a
185 complex (Supplementary Figure 1H).

186

187 **GORAB domains are stable entities**

188 To better understand the nature of the GORAB puncta (membrane domains), we
189 investigated their dynamics. GFP-tagged GORAB was stably expressed at low
190 levels and FRAP was performed. As shown in Fig 3A, recovery of GFP-GORAB
191 fluorescence was slow when compared to the GFP-tagged Golgi enzyme GalNac-
192 T2. This result indicates that GORAB is stably associated with the domains, and
193 therefore that the domains themselves are stable entities. In contrast, recovery
194 of GFP-tagged Scyl1 in the Golgi region was much faster, indicating that Scyl1 can
195 rapidly exchange with the membrane (Fig 3A and Supplementary Figure 2). Co-
196 expression with mApple-GORAB decreased the rate of exchange of GFP-Scyl1
197 with the membrane, in addition to increasing the immobile fraction
198 (Supplementary Figure 2). However the rate of GFP-Scyl1 exchange remained
199 significantly faster than that of GORAB (see Fig 3A), supporting the view that
200 Scyl1 rapidly exchanges with stable GORAB domains. The GORAB domains

201 persist upon depletion of Scyl1 (Fig 3B) or treatment of cells with brefeldin A
202 (BFA) to remove Golgi-associated ARF and COPI (Fig 3C), indicating that the
203 domains can form independently of Scyl1, Arf and COPI.

204

205 **GO disease mutations disrupt Scyl1 binding and GORAB domains**

206 A number of disease-causing mutations have been described in the GORAB
207 sequence, including several missense mutations [22,38,39]. Two recently described
208 mutations identified in a compound heterozygous GO patient (F8L and K190del),
209 are of particular interest considering that neither mutation affects gross folding
210 of GORAB or its targeting to the Golgi apparatus (Gopal-Kothandapani et al, in
211 preparation) (Fig 4A). These mutations must therefore affect another aspect of
212 GORAB function. Pull-down experiments indicated that the F8L mutation does
213 not affect binding of GORAB to Arf1, Arf5, or Rab6, or the ability of GORAB to
214 self-associate (Fig 4B). It does, however, greatly diminish binding to Scyl1,
215 consistent with its location in the N-terminal Scyl1-binding region of GORAB (Fig
216 4B). Surface plasmon resonance with purified proteins indicated high affinity
217 binding of wild-type GORAB to Scyl1 (kD of 0.52 nM), with the F8L mutant
218 demonstrating a complete loss of binding (Fig 4C and Supplementary Figure 3A).
219 The pathogenic effect of the F8L mutation indicates that the GORAB-Scyl1
220 interaction is physiologically important.

221 Like F8L, the K190del mutant can also bind to Arf1, Arf5 and Rab6,
222 although in this case binding to the Arfs is enhanced compared to wild-type
223 GORAB (Fig 4B). Binding to Scyl1 is not markedly affected by the K190del

224 mutation, as indicated by pull-down (Fig 4B) and surface plasmon resonance
225 (Fig 4C), which gives an identical binding affinity to wild-type GORAB (kD=0.52
226 nM) (Supplementary Figure 3B). However, strikingly, there is a complete loss of
227 GORAB self-association in the K190del mutant, as indicated by pull-down (Fig
228 4B). The loss of GORAB self-association with the pathogenic K190del variant
229 indicates this property of the protein is of physiological importance. Expression
230 of the F8L and K190del variants in cells indicated that while the F8L still
231 localizes to discrete domains, the K190del is unable to do so, and is evenly
232 distributed through the *trans*-Golgi (Fig 4D). Hence, self-association of GORAB is
233 required for the assembly of the GORAB puncta. Together, the results indicate
234 that both Scyl1 binding and oligomerization for stable domain assembly are
235 required for full functionality of GORAB *in vivo*.

236

237 **GORAB and Scyl1 cooperate for COPI binding at *trans*-Golgi**

238 The ability of GORAB to form stable domains that also contain Scyl1, which in
239 turn can bind to COPI, led us to propose that GORAB forms a scaffold that
240 promotes COPI assembly at the *trans*-Golgi. To test this hypothesis, wild-type
241 GORAB or mutants deficient in Scyl1 binding (F8L) or oligomerization (K190del)
242 were expressed in cells and the stability of COPI membrane association assessed
243 by treating cells with BFA. As shown in Fig 4E and F, over–expression of wild-
244 type GFP-tagged GORAB stabilized COPI association with the Golgi membranes,
245 indicated by the retention of COPI in the perinuclear region following 10 min
246 treatment with BFA. This is in contrast to control cells, where COPI was
247 completely cytosolic at the same time point. The stabilization of COPI at the Golgi

248 was lost with the F8L or K190del mutants, indicating that both Scyl1 binding and
249 oligomerization of GORAB are required to elicit this effect (Fig 4F and
250 Supplementary Figure 4A).

251 To further test the hypothesis, Scyl1 was also over-expressed in cells. The
252 expression of Scyl1 stabilized membrane association of COPI upon BFA
253 treatment, which was evident both in puncta within the Golgi region that
254 correspond to GORAB domains and in more peripheral puncta likely
255 corresponding to the ERGIC (Fig 4G-I). The ΔNTK Scyl1 mutant that cannot bind
256 to GORAB, and the ΔCT mutant that cannot bind COPI, failed to stabilize COPI at
257 the Golgi (Fig 4H and Supplementary Figure 4B), indicating that Scyl1 must
258 interact with GORAB and COPI to elicit this effect. Interestingly, the ΔNTK mutant
259 was still able to stabilize COPI association with the ERGIC (Supplementary Figure
260 4B), indicating it can stabilize COPI at this compartment independently of
261 GORAB, consistent with the existence of at least two functionally distinct pools of
262 Scyl1 in the secretory pathway. This view is further supported by fact that Scyl1
263 recruitment to the Golgi, but not the ERGIC, requires binding to GORAB, as
264 shown by the lack of Golgi localization of the ΔNTK mutant in untreated cells
265 (Supplementary Figure 4C), and the loss of Golgi-associated Scyl1 in GORAB
266 deficient fibroblasts (Supplementary Figure 4D). Over-expression of GORAB or
267 Scyl1 had no effect upon membrane recruitment or BFA-sensitivity of the *trans*-
268 Golgi Arf-dependent clathrin adaptor complex AP1, as indicated by staining for γ-
269 adaptin (Supplementary Figure 5A and B). Together, these results indicate that
270 GORAB and Scyl1 associate to selectively stabilize recruitment of COPI at the
271 *trans*-Golgi.

272

273 **GORAB and Scyl1 are sufficient for COPI membrane binding**

274 We next wanted to test whether GORAB and Scyl1 are sufficient to drive COPI
275 membrane recruitment. For this purpose GORAB was relocated to mitochondria
276 using a previously described inducible targeting method [40,41]. In this approach,
277 GORAB containing a C-terminal FKBP tag was expressed in cells co-expressing
278 mitochondrial targeted FRB, which binds to FKBP only in the presence of
279 rapamycin, allowing inducible relocation of GORAB to mitochondria upon
280 rapamycin addition (Fig 5A). For these experiments we used the K190del
281 mutant, which gave a clearer mitochondrial targeting, although similar results
282 were obtained with wild-type GORAB. Cells were also treated with nocodazole to
283 depolymerise microtubules and disperse the Golgi, giving a clearer readout [41]. In
284 the absence of rapamycin, GORAB was localized to Golgi elements, where it co-
285 localized with GFP-Scyl1, as expected (Fig 5B). Upon addition of rapamycin,
286 GORAB was efficiently relocated to mitochondria, and co-expressed GFP-Scyl1
287 (Fig 5B), or endogenous Scyl1 (Fig 5C), also redistributed to the GORAB-positive
288 mitochondrial membrane. Golgi markers were absent from mitochondria under
289 these conditions, excluding the possibility of gross distribution of Golgi elements
290 (Supplementary Figure 6A). Endogenous COPI was partially localized to the
291 GORAB and GFP-Scyl1 containing mitochondria, although there remained a
292 significant amount in cytoplasmic puncta, likely corresponding to the ERGIC and
293 dispersed Golgi elements (Fig 5D). This result suggested that GORAB and Scyl1
294 can recruit COPI to mitochondria. To further assess this possibility, cells were
295 treated with BFA to remove COPI from the Golgi and ERGIC. Under these

296 conditions, there was almost complete redistribution of COPI to the
297 mitochondria (Fig 5D). Mitochondrial recruitment of COPI was not obvious in the
298 absence of GFP-Scyl1 co-expression (Supplementary Figure 6B), likely due to the
299 limiting amounts of endogenous Scyl1 in the cell compared to COPI [42]. Together,
300 the results indicate that co-expressed GORAB and Scyl1 are sufficient to recruit
301 COPI to the mitochondrial membrane. Moreover, it shows that COPI can be
302 recruited to the GORAB-Scyl1 complex in the absence of membrane-associated
303 Arf, which is further supported by the absence of mitochondrial Arf under
304 conditions where COPI is recruited there (Supplementary Figure 6C). As
305 expected, Scyl1 deficient in GORAB (ΔNTK) binding failed to associate with
306 mitochondria and recruit COPI, while the COPI binding mutant (ΔCT) was
307 recruited to mitochondria but failed to recruit COPI (Supplementary Figure 7).
308 Thus, GORAB recruits Scyl1, which in turn recruits COPI. In the same assay, we
309 failed to observe mitochondrial relocation of AP1 (Supplementary Figure 8A).
310 We also failed to observe GORAB-dependent mitochondrial recruitment of GFP-
311 tagged Scyl2 or Scyl3, the latter of which has recently been proposed to function
312 redundantly with Scyl1 [43] (Supplementary Figure 8B). Lack of interaction
313 between GORAB and Scyl3 was further confirmed in a pull-down experiment
314 (Supplementary Figure 8C). Thus, GORAB selectively interacts with Scyl1, and
315 the GORAB-Scyl1 complex is sufficient to drive selective membrane association
316 of COPI (Supplementary Figure 8D).

317 Liposome binding experiments further supported a role for Scyl1 in
318 promoting COPI association with membranes. As shown previously [19,44],
319 incubation of synthetic liposomes with purified coatomer and Arf1 leads to

320 recruitment of both proteins to the liposome membrane in a GTP-dependent
321 manner (Fig 6A). Scyl1 is also recruited to liposomes in the presence of Arf1 (Fig
322 6A), consistent with its ability to bind directly to Arf1-GTP (Supplementary
323 Figure 1G). When Scyl1 is added to liposomes in the presence of Arf1 and
324 coatomer, Arf1 recruitment is not significantly altered, but recruitment of
325 coatomer is increased nearly two-fold (Fig 6B and C). Scyl1 is therefore able to
326 enhance COPI recruitment to membranes in a manner independent of Arf1
327 association.

328

329 **Loss of GORAB causes defective protein glycosylation**

330 COPI is required for recycling of Golgi resident proteins, including the numerous
331 enzymes that process glycans on cargo proteins and lipids as they transit the
332 Golgi apparatus [45]. We therefore hypothesized that loss of GORAB would cause
333 altered processing of cargo proteins due to impaired enzyme recycling. To test
334 this possibility, dermal fibroblasts from wild-type or GO donors were subjected
335 to *N*-glycomics analysis by mass spectrometry. This revealed a reduction in
336 abundance of complex terminally sialylated glycans in the GO fibroblasts
337 compared to wild-type controls, with a small reciprocal increase in their
338 galactose terminated precursors, suggesting a deficit in addition of terminal
339 sialic acid (NeuAc) residues in the GO cells (Fig 7A). The deficit in terminal
340 sialylation was confirmed using lectins. Immunofluorescence microscopy with
341 fluorescently tagged *Maackia Amurensis* Lectin I (MALI) and *Sambucus Nigra*
342 (SNA) lectins that specifically recognize sialic acid attached to terminal galactose
343 or GalNAc via an α-2,3 linkage (MAL) or α-2,6 linkage (SNA) respectively,

344 showed a significant reduction in SNA staining in GO fibroblasts compared to
345 controls (Fig 7B and C). In contrast, MAL staining was comparable between
346 control and GO cells, indicating a preferential deficit in α-2,6 linkage of sialic acid
347 to terminal galactose. Reduced SNA lectin staining was also evident by FACS
348 analysis of GO compared to control fibroblasts (Fig 7D). To more directly assess
349 glycosylation efficiency cells were metabolically labeled with alkyne-tagged
350 NeuAc precursor ManNAl, which allows fluorescence detection of sialic acid
351 incorporation into glycoproteins within living cells [46]. GO cells incorporated less
352 fluorescently tagged sialic acid at the *trans*-Golgi compared to wild-type controls,
353 indicating reduced sialylation upon loss of GORAB (Fig 7E and F).

354 To assess whether loss of GORAB also caused altered glycosylation *in vivo*,
355 skin samples were obtained from a GORAB-deficient knockout mouse [47] and
356 analyzed by glycomics. The analysis revealed a striking reduction in complex *N*-
357 glycans, which includes the species with terminal sialic acid residues (Fig 7G),
358 and a reciprocal increase in $Mann_5$ oligomannose species (Fig 7G). Blotting of
359 mouse skin samples with lectins corroborated the mass spectrometry data,
360 showing a reduction in high molecular weight species detected by the SNA and
361 E-PHA lectins, which label α-2,6 linked terminal sialic acid and complex *N*-glycan
362 chains respectively (Fig 7H and I). Loss of GORAB therefore leads to perturbation
363 of protein glycosylation in the Golgi apparatus, with a reduced abundance of
364 complex and terminally modified glycoproteins. The phenotype is evident *in*
365 *vitro* but appears to be more penetrant *in vivo.*

366

367 **Mislocalization of sialyltransferase upon loss of GORAB**

368 The glycomics and lectin data suggested a deficit in recycling of enzymes
369 involved in generating complex terminally modified glycan species, most
370 strikingly terminal α-2,6 sialylation, in GO cells. Defective recycling would be
371 expected to cause a shift in enzyme distribution to later Golgi compartments, or
372 even to post-Golgi compartments. Due to the lack of reagents to label
373 endogenous ST6GAL1 and ST6GALII, we generated a HeLa cell line stably
374 expressing HRP fused to ST6GALI (designated ST-HRP). This fusion allows
375 localization to be performed at high resolution using cytochemical staining
376 followed by electron microscopy, and has previously been used to track *trans*-
377 Golgi morphology during the cell cycle [48]. In control cells treated with luciferase
378 siRNA (Fig 8A), ST-HRP was predominantly localized to the *trans*-most cisterna
379 of the Golgi stack, with some additional signal present in adjacent tubulo-
380 vesicular profiles corresponding to the *trans*-Golgi network (TGN) (Fig 8B and
381 C). Upon depletion of GORAB (Fig 8A), ST-HRP exhibited a shift in distribution
382 towards the TGN, as well as additional circular profiles within the vicinity of the
383 TGN (Fig 8B and C). This effect upon ST-HRP distribution was not due to a
384 change in Golgi morphology, which was unaffected by GORAB depletion in these
385 cells (Fig 8B). Like GORAB, depletion of Scyl1 (Fig 8A) also resulted in a shift of
386 ST-HRP to later compartments (Fig 8B and C). As a positive control, we also
387 depleted the Cog3 subunit of the COG complex (Fig 8A), which is a tethering
388 complex required for COPI-dependent Golgi enzyme recycling [45]. As reported
389 previously [49], Cog3 depletion caused extensive vesiculation of Golgi membranes,
390 with a certain proportion of the vesicles containing ST-HRP, indicating a failure
391 to tether *trans*-Golgi derived vesicles (Fig 8B and C). In summary, these results
392 reveal that both GORAB and Scyl1 are required to maintain a normal ST-HRP

393 distribution within the Golgi apparatus, as would be expected if they functioned
394 together in COPI-mediated enzyme recycling at the *trans*-Golgi.

395

396 **Altered Golgi morphology upon loss of GORAB**

397 Although the Golgi appeared morphologically normal in GORAB-depleted HeLa
398 cells, we next wanted to determine whether the Golgi organization is altered by
399 loss of GORAB in dermal fibroblasts, which represent a better model of the
400 human disease. Dermal fibroblasts secrete high amounts of extracellular matrix
401 proteins and may therefore be more sensitive to perturbation of intra-Golgi
402 traffic than HeLa cells, which have a lower secretory capacity. As expected, in
403 control fibroblasts, the Golgi apparatus formed a characteristic Golgi stack, with
404 clearly discernable cisternae surrounded by small spherical profiles that likely
405 correspond to transport vesicles (Fig 8D). Although some cisternal distensions
406 were observed in control fibroblasts, in GO fibroblasts, the distensions were
407 larger and more numerous, and were restricted to one side of the Golgi, most
408 likely the TGN and the *trans*-most cisternae, where they were often present at
409 the rims (Fig 8D and E). Hence, GORAB appears to be required to maintain
410 normal organization of the *trans*-Golgi in dermal fibroblasts, which is consistent
411 with a role for the protein in intra-Golgi trafficking at this compartment.

412

413 **Discussion**

414 In this study we have identified GORAB as a factor in COPI trafficking at the Golgi
415 apparatus. Together with the COPI-binding protein Scyl1 it scaffolds COPI
416 assembly at discrete regions (domains) of the *trans*-Golgi. The GORAB domains
417 are functionally important as their loss, or their inability to interact with Scyl1
418 and therefore COPI, causes GO in humans. The GORAB domains are restricted to
419 the *trans*-Golgi despite COPI being more abundant at the *cis*-side of the Golgi
420 apparatus and the ERGIC. This observation suggests that COPI requires an extra
421 degree of organization to function efficiently at the *trans*-Golgi compared to
422 earlier in the secretory pathway. The TGN is a complex compartment with
423 multiple functional domains [50,51]. Moreover, the predominant Arf binding coat
424 proteins at the TGN are AP1 and the GGAs [51]. Hence, GORAB may improve the
425 efficiency of COPI assembly at the TGN by recruiting Scyl1 and GTP-loaded Arf1,
426 both of which bind COPI, into discrete domains (Fig 8F). The high local
427 concentration of Scyl1 and Arf1 in these domains would allow the coincident
428 detection of both proteins, and favour the selective concentration of COPI, at the
429 expense of AP1. Because GORAB and Scyl1 are oligomers, recruitment of COPI is
430 likely to be further enhanced by the multivalent nature of the interactions
431 between these proteins. The ability of Scyl1 to bind two distinct sites in COPI
432 also suggests that it may contribute to the coat assembly process by potentially
433 bridging individual coatomer complexes [33].

434 GORAB is required for recruitment of Scyl1 to the *trans*-Golgi. However,
435 Scyl1 is also present at the *cis*-Golgi and ERGIC [34], and recruitment of Scyl1 to
436 these earlier compartments is independent of GORAB. There are therefore two

437 distinct pools of Scyl1 in the cell, a GORAB-dependent *trans*-Golgi pool and a
438 separate GORAB-independent *cis*-Golgi/ERGIC pool. How Scyl1 is recruited to
439 the *cis*-Golgi and ERGIC is currently unknown. We have shown that it binds to
440 GTP-loaded Arf1, but the persistent association of Scyl1 with the ERGIC upon
441 BFA treatment indicates that another binding factor must exist [34]. A potential
442 candidate is FTCD/58K, which can bind Scyl1 [52], but this protein appears to be
443 absent from the ERGIC, suggesting that another, as yet unidentified, protein
444 recruits Scyl1 to this compartment. Regardless of how Scyl1 is recruited to the
445 membrane, its role in promoting COPI assembly appears to be conserved at the
446 different locations. Scyl1 may therefore act as a COPI 'receptor', as has been
447 proposed for p23 [15,19]. These proteins may even act in tandem at the *cis*-Golgi
448 and ERGIC to promote COPI recruitment, whereas at the *trans*-Golgi, Scyl1
449 presumably acts independently of p23, which is not present there.

450 The other two members of the Scyl family, Scyl2 and Scyl3, are both also
451 present at the Golgi apparatus [43,53,54]. Scyl2, also known as CVAK104, functions as
452 a clathrin adaptor at the *trans*-Golgi, and participates in sorting of SNAREs into
453 clathrin-coated vesicles that shuttle between the TGN and endosomes [53,55]. Its
454 function is therefore distinct from that of Scyl1. In contrast to Scyl2, but similar
455 to Scyl1, Scyl3 appears able to bind COPI, and knockout studies in mice indicate
456 functional redundancy between the Scyl1 and Scyl3, at least in neurons [43]. Hence,
457 these proteins may share overlapping functionality. However, our results, which
458 show that neither Scyl2 nor Scyl3 can bind GORAB, indicate that Scyl1 has a
459 function distinct from that of Scyl3, namely in the scaffolding of COPI into
460 discrete membrane domains at the *trans*-Golgi. It will be interesting to further

461 analyze the role of Scyl3 in COPI traffic, and also to compare how the loss of
462 Scyl1 or Scyl3 affects COPI trafficking in different cell types.

463 Loss of Scyl1 in humans manifests as CALFAN syndrome, which causes
464 neurodegeneration, similar to that seen in Scyl1-deficient mice [56] and liver
465 failure, with some patients also showing skeletal abnormalities [57,58]. The
466 different symptoms in CALFAN syndrome compared to GO could be explained by
467 Scyl1 functioning earlier in the secretory pathway, at the ERGIC and *cis*-Golgi, in
468 addition to its GORAB-specific function at the *trans*-Golgi [34,52]. This is likely to
469 differentially affect secretory traffic, which may be further complicated by
470 differences in the extent to which loss of Scyl1 or GORAB affects trafficking in
471 different cell types, also considering the possible functional overlap with Scyl3 [43].
472 A better understanding of the disease mechanisms in CALFAN and GO patients
473 will help resolve these issues.

474 We observed impairment of protein glycosylation in GO cells and in a
475 GORAB-knockout mouse. Thus, GO can be considered as a congenital disorder of
476 glycosylation (CDG) [59]. Type II CDGs are associated with defects in glycan
477 processing [59], and we propose that GO is included in this category of CDGs.
478 Interestingly, several type II CDGs are due to mutations in the COG complex,
479 which is required for tethering of intra-Golgi transport vesicles [60]. Loss of COG
480 leads to impaired enzyme recycling, resulting in improper cargo protein
481 glycosylation [45]. Although there is some variability in the severity of the
482 phenotype depending upon the nature of the COG mutation, CDGs due to COG
483 mutations tend to be more severe than GO [45], reflecting the more widespread
484 role for COG in enzyme recycling throughout the Golgi stack. Loss of GORAB

485 tends to cause a milder phenotype, as would be expected from its exclusive role
486 in the recycling of *trans*-Golgi enzymes. Interestingly, wrinkled and lax skin, as
487 seen in GO, is also evident in autosomal recessive cutis laxa type 2 (ARCL2),
488 which is caused by mutation of the ATP6V0A2 subunit of the vacuolar ATPase
489 [61]. The vacuolar ATPase is required maintain an acidic intra-luminal Golgi pH
490 that is optimal for cargo protein glycosylation. Hence, the increased
491 intraluminal Golgi pH upon loss of ATP6V0A2 is thought to cause impaired
492 glycosylation and trafficking of secretory cargoes [61,62]. As seen in GO, sialylation
493 of cargo proteins is particularly affected by loss of ATPV0A2 [61], suggesting with
494 a common pathogenic mechanism in both ARCL2 and GO.

495 Although we show here that the modification of *N*-linked glycans is
496 impaired by loss of GORAB, it is likely that *trans*-Golgi enzymes involved in the
497 modification and processing of O-linked glycan chains, such as those found in
498 proteoglycans, is also affected. Indeed, our analysis of the small leucine-rich
499 proteoglycans (SLRPs) decorin and biglycan in the skin and bone of GORAB-
500 deficient mice has shown a dramatic reduction in the degree of glycanation of
501 these proteins [47]. SLRPs are abundant proteins of the extracellular matrix, where
502 they associate with collagen to stabilize matrix assembly [63]. Loss of SLRPs causes
503 pathological changes in skin, skeleton, and cardiovascular tissues in mouse
504 models and human patients [63]. SLRPs are particularly sensitive to mutation of
505 enzymes involved in GAG chain synthesis [64-67], and defects in several of these
506 enzymes cause connective tissue disorders with similar clinical features to those
507 seen in GO [64,66,67]. It is therefore likely that impaired glycanation of decorin and

508 possibly other proteoglycans, due to defective recycling of glycanation enzymes,
509 contributes to the skin and bone phenotypes seen in GO.

510 GORAB is widely expressed in the body [22], and we show here that it
511 functions in a universally important process, namely COPI-mediated intra-Golgi
512 trafficking. This raises the question as to why GO is manifest in the skin and
513 bones. One possibility is that loss of GORAB is compensated for by another
514 protein in most tissues. However, GORAB does not have any obvious functional
515 homologues, arguing against this possibility. Rather, we favour the idea that the
516 tissues most affected by loss of GORAB i.e. skin and bone, are those that are most
517 sensitive to impaired glycosylation and glycanation of cargo proteins. These
518 tissues comprise large amounts of extracellular matrix, and matrix assembly and
519 maintenance are susceptible to impairment of matrix protein glycosylation and
520 glycanation. Hence, loss of GORAB manifests primarily in these matrix-rich
521 tissues. We have shown that decorin is a relevant substrate in this regard [47], but
522 other matrix proteins are also likely to be affected, especially those that undergo
523 extensive sialylation or glycanation.

524 A recent study using both *Drosophila* embryos and human tissue culture
525 cells has uncovered a role for GORAB in centriole duplication, which is distinct
526 from its function at the Golgi apparatus [31]. This suggests that centriolar defects
527 may contribute to the GO phenotype. However, analysis of a pathogenic GO
528 mutation that disrupts Golgi targeting (A220P) showed no effect upon GORAB
529 function at the centriole. This finding is consistent with Golgi dysfunction being
530 the primary cause of GO, although we cannot exclude an involvement of
531 centriolar defects in GO pathology, possibly through defects at the cilium [30,31].

532 Interestingly, interference with Golgi targeting of *Drosophila* Gorab resulted in a
533 spermatogenesis defect very similar to that seen in COPI deficient flies,
534 consistent with a functional association between GORAB and COPI being
535 conserved in evolution [31,68].

536

537 **Methods**

538 **Reagents and antibodies.** Reagents were obtained from Sigma-Aldrich, Merck,
539 or Thermo Fisher Scientific unless otherwise specified. Primary antibodies used
540 in this study are detailed in Supplementary Table 2. Alexa 488-conjugated
541 streptavidin, Alexa 488-, 546-, 55-, 594- and 647-conjugated, and Cy3- and Cy5-
542 conjugated secondary antibodies were from Molecular Probes (Thermo Fisher
543 Scientific) and from Jackson ImmunoResearch Laboratories, respectively.
544 Horseradish peroxidase–conjugated secondary antibodies were from Sigma.
545 HRP-conjugated streptavidin was from GenScript.

546

547 **Molecular biology**. GORAB and Scyl1 cDNA sequences were obtained from the
548 I.M.A.G.E. Consortium (Source Biosciences). All amino acid positions of GORAB
549 mentioned in this study refer to the 369 amino acid. protein, which originates
550 from the ENST00000367763.7 transcript using the second predicted start codon,
551 which is the correct translation start site [22,25]. Using standard molecular biology
552 techniques full-length and truncated GORAB and Scyl1 sequences were
553 subcloned into pEGFP-C3 (Clontech Laboratories), pGADT7 and pGBKT7 (BD
554 Biosciences), pFAT2 (a modified pGAT2 vector) and pMAL-C2 (New England

555 Biolabs) for mammalian expression, yeast two-hybrid analysis, and bacterial
556 expression, respectively. Missense patient mutations were introduced by site-
557 directed mutagenesis performed using PfuTurbo DNA polymerase adapted from
558 the Quikchange site-directed mutagenesis method (Agilent Technologies). To
559 make GORAB-mycFKBP constructs, GORAB and myc-FKBP fragments were
560 inserted into pcDNA3.1 vector (Invitrogen). Vectors encoding GST-tagged
561 Δ14Arf1 (Q71L and T31N) were a gift from Dr. Sean Munro (Laboratory of
562 Molecular Biology, Cambridge, UK). Arf1 was subcloned into pET24a (Merck)
563 and pcDNA3.1 HA-tag (Invitrogen). GST-tagged Δ14Arf3-GTP (Q71L] and GDP
564 [T31N), Δ14Arf4-GTP (Q71L] and GDP [T31N) and Δ14Arf5-GTP (Q71L] and GDP
565 [T31N) were subcloned from vectors obtained from Dr. Elizabeth Sztul
566 (University of Alabama, Birmingham, USA). Vectors encoding GST-tagged γ-1
567 appendage, Rab6-GTP (Q72L] and GDP [T27N), Bet1 and syntaxin-1 were
568 described previously [69-71]. pSRα-SialylT-HRP plasmid containing cytoplasmic tail,
569 transmembrane domain and part of luminal domain of ST6GAL1 fused with
570 horseradish peroxidase (HRP) was previously described [48]. Mito-FRB plasmid
571 was a gift from Dr. Stephen Royle (University of Warwick, Warwick, UK). Vector
572 encoding GFP-Scyl2 was obtained from Dr Ernst Ungewickell (Hannover Medical
573 School, Hannover, Germany). Vector encoding Scyl3-myc was obtained from Dr.
574 Rick Thorne (Newcastle, New South Wales, Australia). Scyl3 was subcloned into
575 pEGFP-N3 (Clontech Laboratories). Primer sequences used for molecular cloning
576 are described in Supplementary Table 3.

577

578 **Cell culture, transfection, RNAi, and drug treatments**. Written informed
579 consent for molecular studies was obtained from control and affected individuals
580 or from their legal representatives. Dermal fibroblasts were obtained by
581 standard punch biopsy. All studies on patient fibroblasts were carried out in
582 accordance with local ethical regulations, with approval from the University of
583 Manchester Research Ethics Committee. Patient fibroblasts were also obtained
584 from the Cell Line and DNA Bank from Patients Affected by Genetic Diseases
585 (Genova, Italy, codes: FFF0631984 and FFF0731991). All cells were grown at
586 37˚C and 5% CO_2. HeLa (ATCC CCL-2), HeLaM (RRID:CVCL_R965), HEK298 (Cell
587 Biolabs, LTV-100) and human dermal fibroblasts were grown in Dulbecco's
588 Modified Eagle's medium (DMEM) supplemented with 10% (vol/vol) fetal
589 bovine serum (FBS), 1 mM L-glutamine and penicillin-streptomycin mix. Non-
590 essential amino acid solution was added to human skin fibroblasts, while HeLa
591 cells stably expressing ST6GALI-HRP (ST-HRP) and HeLa cells stably expressing
592 GFP-GalNac-T2 (Dr. Brian Storrie, University of Arkansas for Medical Sciences,
593 Little Rock, AK) were supplemented with 1 mg/mL and 0.5 mg/mL G418,
594 respectively. hTERT-RPE-1 cells (ATCC) were grown in 1:1 mix of Ham's F12 and
595 DMEM supplemented with 10% (vol/vol) FBS, 1 mM L-glutamine, penicillin-
596 streptomycin mix and 10 μM hygromycin B. Transient transfection of plasmid
597 DNA was performed using FuGene HD (Promega) according to the
598 manufacturer's instructions and cells were assayed 24–48 h post-transfection.
599 For RNAi interference, HeLa ST-HRP cells were transfected with 20 nM siRNA
600 duplexes using INTERFERin (Polyplus Transfection) according to the
601 manufacturer's instructions and were analyzed 72 h post-transfection. GORAB
602 was targeted with ON-TARGETplus SMARTpool (pool of four siRNAs; L-016142;

603 sense: AGCUAGAUAUACAGCGCAA, CAACAACUUCAGCGAGAAA,
604 CAACAAGAACAACGGCUAA and CCAUGAAACUAAAGCGGAU), Scyl1 with ON-
605 TARGETplus SMARTpool (pool of four siRNAs; L-005373, sense:
606 GCUCUGCGGUCUCACUGUA, GAAGUGGUCAGCAGACAUG,
607 CAAGUGAGCCGUGCUAGUC and GCUACACCAGAUCGUGAAA), and Cog3 with a
608 previously described siRNA (sense: AGACUUGUGCAGUUUAACA, [49], all purcahsed
609 from Dharmacon (Thermo Fisher Scientific). Luciferase siRNA (GL2; Eurogentec,
610 sense: CGUACGCGGAAUACUUCGA) was used as negative control. For the
611 mitochondrial relocation assay, HeLaM cells were treated with 2.5 µg/mL
612 nocodazole for 2 h, followed by addition of 1 µM rapamycin (Calbiochem) for 3 h
613 to induce targeting of GORAB K190del-mycFKBP onto mitochondrial outer
614 membranes. In some experiments cells were incubated with 5 µg/mL brefeldin A
615 (Sigma) for an indicated time period.

616

617 **Lentivirus production.** HEK293 cells were seeded on 10 cm dishes 24 h prior to
618 transfection. For each dish, 6 µg of pXLG3-GORAB plasmid, 4.5 µg of psPAX2
619 packaging plasmid and 3 µg of pM2G envelope plasmid were transfected into
620 HEK293 cells using 27 µL of polyethylenimine mix (1 mg/mL in 150 mM NaCl)
621 and antibiotic-free medium. 6-8 h after transfection the medium was replaced.
622 The following day transfected cells were supplemented with 100 µl of 1M
623 sodium butyrate (Merck) for 6-8 h and the medium was replaced. 72 h after the
624 initial transfection, the virus-containing medium was collected and precleared by
625 centrifugation (10 min, RT at 2,700 xg in Rotofix 32A centrifuge (Hettich

626 Centrifuges)) and the supernatant was filtered through a 0.44 μm syringe-driven
627 filter unit. 1-3 mL of virus-containing medium was used for cell transduction.

628

629 **Protein-binding assays.** Cells were lysed in HMNT buffer (20 mM HEPES-KOH
630 pH 7.4, 5 mM $MgCl_2$, 0.1 M NaCl, 0.5% (wt/vol) Triton X-100) supplemented with
631 protease inhibitor cocktail (Calbiochem) and pre-cleared by centrifugation at
632 16,000 xg for 15 min at 4˚C in a microfuge. For pull-down experiments, 40 μg of
633 GST-tagged bait protein bound to 20 μL of glutathione resin was incubated with
634 cell lysate (300-500 μL of lysate for exogenously expressed proteins; 2-3 mg of
635 sHeLa cell lysate for endogenously expressed proteins) for 4 h at 4˚C with
636 agitation. Bound proteins were eluted in SDS sample buffer analyzed by SDS-
637 PAGE with Western blotting. Proteins from rat liver Golgi membranes [72], were
638 extracted in HKMT buffer (20 mM HEPES-KOH pH 6.8, 160 mM KOAc, 1 mM
639 $MgCl_2$, 0.5% (wt/vol) Triton X-100), pre-cleared by centrifugation at 55 000 xg
640 for 10 min at 4˚C and the supernatant was used for pulldown reactions, as
641 described above. For direct binding assays between GST-tagged and MBP-tagged
642 proteins, 20 μg of GST-tagged bait protein bound to 20 μL of glutathione resin
643 was incubated with 20 μg MBP-tagged protein in HMNT buffer supplemented
644 with 100 μg/ml bovine serum albumin for 4 h at 4˚C with agitation. Bound
645 proteins were eluted from the glutathione beads with elution buffer (50 mM
646 Tris-Cl pH 8.1, 25 mM reduced glutathione) for 10 min, followed by
647 trichloroacetic (TCA) precipitation and analyzed by SDS-PAGE with Western
648 blotting or Coomassie blue staining. Uncropped versions of Western blots are
649 shown in Supplementary Figure 9.

650

651 **Surface plasmon resonance.** Experiments were performed using the ProteOn
652 XPR36 instrument (Bio-Rad Laboratories) using the high capacity GLH chip (Bio
653 Rad). Running buffer was 150 mM NaCl, 10 mM HEPES, 0.02% (w/v) Tween-20,
654 pH 7.4. Two channels were activated with 250 μL of 25 mM N-ethyl-N′-(3-
655 dimethylaminopropyl) carbodiimide (EDC) and 8 mM sulfo-N-
656 hydroxysuccinimide (sulfo-NHS) at a flow rate of 30 μL/min. Anti-MBP antibody
657 was bound to both channels to a final level of approx. 16000 response units (RU).
658 MBP-tagged Scyl1 was then captured on the second channel only to a final level
659 of 3000 RU. Binding of GST-tagged GORAB variants to both channels at 30 nM
660 concentration and a flow rate of 100 μL/min was allowed to occur for 120 s
661 followed by 600 s disassociation, using the first channel as a reference. All
662 binding sensorgrams were collected, processed and analyzed using the
663 integrated ProteOn Manager software (Bio-Rad Laboratories).

664

665 **Liposome recruitment assay.** All lipids were purchased from Avanti Polar
666 Lipids. To make 3 mM final 'Golgi lipid' mixture in $CHCl_3$ the following lipids
667 were used: 43 mol% phosphatidylcholine (PC) from bovine liver, 19 mol%
668 phosphatidylethanolamine (PE) from bovine liver, 5mol% phosphatidylserine
669 (PS) from bovine brain, 10 mol% phosphatidylinositol (PI) from bovine liver, 7
670 mol% sphingomyelin (SM) from bovine brain and 16 mol% cholesterol from
671 wool grease. The liposome suspension was then subjected to five cycles of
672 freezing and thawing using dry ice in isopropanol and 37˚C water bath. For a
673 single experiment, 500 μM liposomes were rehydrated in assay buffer (50 mM

674 HEPES pH 7.2, 120 mM KOAc, 1 mM $MgCl_2$) and sized via extrusion through a
675 polycarbonate filter with a pore size of 200 nm (GE Healthcare). Liposomes were
676 then incubated at 37˚C for 20 min with 10 μM MBP-Scyl1 or MBP-IPIP27A, 10 μM
677 recombinant mouse coatomer isotype γ2ζ1 (CMγ2ζ1; produced in Sf9 insect cells
678 [18]) and 5 μM recombinant N-myristoylated human ARF1 (purified to near
679 homogeneity), some additionally supplemented with 100 μM GTPγS in a final
680 volume of 100 μL. Next, samples were adjusted to 35% (w/w) sucrose, overlaid
681 with 300 μl 30% (w/w) sucrose and buffer and centrifuged for 1 h at 256,000 xg
682 in a SW60 rotor (Beckman Coulter). The top fraction (100 μL) containing
683 liposomes was collected, diluted in 500 μL assay buffer, pelleted in a TLA55 rotor
684 (Beckman Coulter) for 1 h at 91,000 xg and analyzed by SDS-PAGE with Western
685 blotting.

686

687 **Immunofluorescence microscopy.** Cells were grown on glass coverslips and
688 washed twice with PBS prior to fixation in 3% (wt/vol) PFA in PBS for 20 min at
689 RT. Cells were then washed with PBS and the excess of paraformaldehyde was
690 quenched with glycine. The cells were permeabilized by 4 min incubation in
691 0.1% (wt/vol) Triton X-100 in PBS or in 0.05% (wt/vol) SDS in PBS. Cells were
692 incubated with primary antibody solution for 1 h at RT and incubated three
693 times with PBS for 5 min. Then coverslips were incubated for 1 h with secondary
694 antibody solution (often supplemented with 200 ng/mL of the DNA dye Hoechst
695 33342) and incubated three times with PBS for 5 min and twice in ddH_20 for 5
696 min. Coverslips were dried before mounting in Mowiol 4-88 (0.1 M Tris-Cl pH
697 8.5, 10% (wt/vol) Mowiol 4-88, 25% (wt/vol) glycerol). Prepared slides were

698 analysed using an Olympus BX60 upright microscope equipped with a MicroMax
699 cooled, slow-scan CCD camera (Princeton Instruments) driven by Metaview
700 software (University Imaging Corporation). Images were processed using ImageJ
701 software (MacBiophotonics).

702

703 **STED microscopy.** Cells were grown on precision glass coverslips (No. 1.5H;
704 Paul Marienfeld), fixed and stained as described above. Images were collected on
705 a Leica TCS SP8 AOBS inverted gSTED microscope using a 100x/1.40 Plan Apo
706 objective. The confocal settings were as follows, pinhole 1 Airy unit, scan speed
707 400Hz unidirectional and format 2048 x 2048. STED images were collected using
708 hybrid detectors with the following detection mirror settings; Alexa-488: 498-
709 542 nm; Alexa-549: 564-619 nm; Alexa-647:646-713 nm using the 490 nm, 555
710 nm and 635 nm excitation laser lines and 592 nm, 660 nm and 775 nm depletion
711 laser lines, respectively. STED images were collected sequentially and
712 deconvolved using Huygens Professional (Scientific Volume Imaging).

713

714 **Fluorescence recovery after photobleaching (FRAP).** HeLa GFP-GalNacT2,
715 HeLaM GFP-GORAB or HeLaM cells transiently expressing GFP-Scyl1 were grown
716 in 35mm glass bottomed dishes (MatTek Corporation). The medium was
717 changed to CO_2-independent medium supplemented with 10% FBS and 1 mM L-
718 glutamine just before FRAP analysis. Images were acquired using a CSU-X1
719 spinning disc confocal (Yokagowa) on a Zeiss Axio-Observer Z1 microscope with
720 a 150x/1.45 numerical aperture oil immersion TIRF objective (Olympus), Evolve

721 EMCCD camera (Photometrics) and motorized XYZ stage (Applied Scientific
722 Instrumentation). The 488nm laser was controlled using an AOTF through the
723 laserstack (Intelligent Imaging Innovations) allowing both rapid 'shuttering' of
724 the laser and attenuation of the laser power. FRAP was carried out at 37˚C using
725 the FRAP imaging module of the Slidebook application (Intelligent Imaging
726 Innovations). A 5 μm rectangular region of interest (ROI) was defined and
727 photobleached at a high laser power to result in >80% reduction in fluorescence
728 intensity. Recovery was monitored by measuring fluorescence intensity at 3-s
729 intervals for a total period of 3 min. FRAP recovery curves were analyzed using
730 FRAPAnalyser software (http://actinsim.uni.lu/; University of Luxembourg,
731 Luxembourg).

732

733 **Metabolic labeling with alkyne-tagged sialic acid.** *N*-(4-pentynoyl)
734 mannosamine (ManNAl) was synthesized according to optimized procedures [46].
735 Cells were grown in DMEM supplemented with 10% FBS and 1 mM L-glutamine
736 containing 500 μM of ManNAl for 10 h before fixation of cells with 4% (wt/vol)
737 PFA. Cells were permeabilized in PBS with 0.1% Triton X-100 for 4 min and
738 incubated with 100 μL/coverslip of a freshly prepared click solution (100 mM
739 K_2HPO_4, 2.5 mM sodium ascorbate, 150 μM $CuSO_4$, 0.3 mM BTTAA, 10 μM
740 AzidoFluor 545). Copper-catalyzed azide-alkyne [3 + 2] cycloaddition (CuAAC)
741 was performed for 45 min in the dark at room temperature with gentle shaking.
742 Cells were then stained with antibodies as described above. Images were
743 acquired on a Ti inverted microscope (Nikon) using a x60/1.40 Plan Apo
744 objective, Proscan II motorized stage (Prior Scientific) and R6 CCD camera

745 (QImaging). A SpectraX LED light engine (Lumencore), quad dichroic (Semrock)
746 and motorized emission filter wheel (Prior Scientific) with single bandpass
747 filters for FITC, TRITC and Cy5 (Semrock) were used to collect image sequences
748 at each position in the tile. Images were acquired and then aligned and stitched
749 using NIS Elements software (Nikon). These stitched images were then exported
750 as a single TIFF image for further processing in Fiji software. The amount of
751 intra-Golgi incorporated alkyne-tagged sialic acid was measured by comparing
752 fluorescence intensity levels with reference to the Golgi marker TGN46. GORAB
753 staining was employed to discriminate between WT and GO fibroblasts.

754

755 **Immunofluorescence-based lectin-binding assays.** The following method was
756 adapted from Willet *et al.* [73]. Human dermal fibroblasts were grown on glass
757 coverslips to 90% confluency. Cells were rinsed twice with pre-chilled PBS and
758 incubated with it for 15 min in order to prevent endocytosis of glycosylated
759 plasma membrane proteins. Next, cells were incubated in FITC-conjugated
760 *Maackia amurensis* (MAL) or *Sambucus Nigra* (SNA) lectin solution (20 μg/mL;
761 Vector Laboratories) for 20 min in the cold room. Coverslips were washed three
762 times with pre-chilled PBS and incubated with pre-chilled 4% (wt/vol) PFA
763 solution prepared in PBS for 20 min. Cells were washed three times with PBS
764 and excess PFA was quenched by addition of glycine. Coverslips were washed
765 with ddH_20, left at RT to dry and mounted using Mowiol 4-88. Samples were
766 imaged on a Ti inverted microscope (Nikon).

767

768 **Flow cytometry.** Human skin fibroblasts were grown on 10-cm dishes to 100%
769 confluency. Cells were washed with pre-warmed PBS and detached using pre-
770 warmed Accutase (Sigma). Next, cells were washed twice with PBS, resuspended
771 in pre-chilled PBS and incubated for 15 min on ice followed by incubation in
772 *Maackia amurensis* (MAL) or *Sambucus Nigra* (SNA) lectin solution (20 μg/mL;
773 Vector Laboratories) for 30 min at 4˚C. Next, cells were washed three times with
774 PBS, resuspended in 400 μL of ice-cold PBS and analyzed using a Beckman
775 Coulter Cyan ADP flow cytometer with a 488-nm laser. Propidium iodide was
776 added to exclude non-viable cells from the flow cytometry analysis. Data were
777 analyzed using Summit V4.3 software (Beckman Coulter).

778

779 **Electron microscopy.** For morphological analysis, human skin fibroblasts were
780 grown on glass coverslips and flat embedded. Serial thin sections (60 nm) were
781 cut parallel to the coverslip and sections at approximately equal intervals were
782 imaged with Jeol JEM-1400 microscope operated at 80 kV. Images were acquired
783 with Gatan Orius SC 1000B camera. For pre-embedding immuno-EM, cells were
784 fixed with PLP-fixative for 2 h, permeabilized with 0.01% saponin, labeled with
785 anti-GORAB rabbit antibody followed by nano-gold-conjugated anti-rabbit IgG
786 F_{ab}-fragments (Nanoprobes), post-fixed with 1% glutaraldehyde, and quenched
787 with 50 mM glycine. Nano-gold particles were then intensified using the HQ
788 SILVER Enhancement kit (Nanoprobes, Cat.No 2012) followed by gold toning in
789 subsequent incubations in 2% NaAcetate, 0.05% $HAuCl_4$ and 0.3%
790 $Na_2S_2O_3 \bullet 5H_2O$. The cells then were processed for EM and imaged as described
791 above. Peroxidase cytochemistry was performed on HeLa SialylT-HRP cells that

792 were seeded on Aclar coverslips (Agar Scientific) and transfected with control,
793 GORAB, Scyl1 or COG3 siRNAs. 72 h after transfection cells were fixed with 2%
794 (wt/vol) paraformaldehyde, 1.5% (wt/vol) glutaraldehyde solution made in 0.1
795 M sodium cacodylate buffer, pH 7.4 for 20 min at RT. Samples were then washed
796 twice with 0.1 M sodium cacodylate buffer for 3 min and 5 times with 50 mM
797 Tris-buffer, pH 7.6 for 5 min. Samples were incubated in freshly prepared 0.1%
798 (wt/vol) DAB (TAAB Laboratories Equipment) made in 50 mM Tris-buffer, pH
799 7.6 and supplemented with 0.0002% (vol/vol) H_2O_2 for 30 min at RT protected
800 from light. Samples were washed 3 times with 50 mM Tris-buffer, pH 7.6 for 5
801 min and twice with 0.1 M sodium cacodylate buffer for 5 min. Sections were cut
802 with Reichert Ultracut ultramicrotome and observed with FEI Tecnai 12 Biotwin
803 microscope at 100 kV accelerating voltage. Images were taken with Gatan Orius
804 SC1000 CCD camera.

805

806 **Yeast two-hybrid assays.** Yeast two-hybrid assays were performed with the use
807 of the Matchmaker Gold system (Clontech Laboratories). First, bait-containing
808 and prey-containing plasmids were co-transformed into the yeast strain
809 Y2HGold with 500 ng of a bait DNA plasmid and 500 ng of a prey DNA plasmid
810 alongside 50 μg of denatured herring sperm DNA acting as a carrier DNA and
811 plated on double drop-out agar plates (SD/-Leu/-Trp). Three single colonies per
812 test condition were inoculated into 4 mL of liquid SD/-Leu/-Trp medium
813 supplemented with glucose and grown for 2 days at 30˚C with 150 rpm agitation.
814 A 10-μL innoculation loop was used to transfer the liquid yeast culture to a
815 square on a double drop-out (SD/-Leu/-Trp) and quadruple drop-out (SD/-

816 Ade/-His/-Leu/-Trp) agar plates. The plates were incubated at 30°C and growth
817 was monitored for a period of 7 days. SD/-Leu/-Trp agar plate was used as a
818 growth control and the selective growth on the SD/-Ade/-His/-Leu/-Trp agar
819 plate indicated interaction between the bait and the prey.

820

821 **Glycan mass spectrometry**. For profiling of control and GO fibroblasts *N*-
822 glycans were isolated using filter-aided *N*-glycan separation (FANGS).
823 Fibroblasts were grown until they were confluent, the medium was removed and
824 cells were washed 6 times with PBS. Cells were scraped in 1 mL PBS using a cell
825 scraper and and centrifuged at 16,000 xg for 5 min at 4˚C. The cell pellet was
826 dissolved in 10x volume of lysis buffer (4% (wt/vol) SDS, 100 mM Tris, pH 7.6,
827 100 mM DTT) and boiled for 5 min at 95˚C followed by centrifugation at 16,000
828 xg for 5 min at RT. Urea buffer (8M in 100 mM Tris-Cl pH 8.5) was added to
829 supernatants at a 10:1 volume ratio and samples were passed through
830 ultrafiltration membranes (Amicon Ultra-0.5, Merck) by centrifugation at 15,000
831 xg for 10 min at RT. Samples retained above filter membranes were subjected to
832 a series of washes combined with centrifugation at 15,000 xg for 10 min at RT:
833 1) washed twice with 250 µL of urea buffer, 2) incubated with 300 µL of urea
834 buffer supplemented with 40 mM iodoacetamide for 15 min before
835 centrifugation, 3) washed once with 250 µL of 8M urea and 4) washed four times
836 with 250 µL of 50 mM NH_4HCO_3. Filter membranes were subsequently
837 incubated with 8 U of PNGase F in 100 µL of 50 mM NH_4HCO_3 for 16 h at 37˚C
838 followed by centrifugation at 15,000 xg for 15 min at RT and washed twice with
839 250 µL water. Samples above filter membranes containing released N-glycans

840 were transferred to glass tubes and dried in a vaccum centrifuge (Ultraflex
841 Power Technologies). Permethylation of glycans was performed as follows:
842 samples were dissolved in 600 μL of DMSO, supplemented with 25 mg of NaOH
843 and mixed until completely dissolved. Then iodomethane was added in the
844 following manner: 375 μL followed by incubation for 10 min at RT, 375 μL
845 followed by incubation for 10 min at RT and 750 μL followed by incubation for
846 20 min at RT. The reaction was quenched by addition of 1.5 mL of 1 g/mL
847 $Na_2S_2O_3$ solution and 1.5 mL of dichloromethane followed by extensive
848 vortexing. Samples were left undisturbed to allow phase separation and the
849 lower, organic, layer was taken to fresh glass tubes and dried under vacuum.
850 Samples were dissolved in 20 μL of methanol. 2 μL of the sample was mixed with
851 1 μL of 0.5 M sodium nitrate (in 70% methanol) and 2 μL of 20 mg/mL 2,5-
852 dihydroxybenzoic acid (in 70% methanol). 2 μL of this mix was spotted onto a
853 ground steel MALDI target plate (Bruker) and allowed to air dry. Immediately
854 afterwards, 0.2 μL of ethanol was added to the spot and left to air-dry for re-
855 crystallization. Glycans were then permethylated and analyzed by mass
856 spectrometry using a Bruker Daltonics ultraflex III TOF/TOF mass spectrometer
857 equipped with a Smartbeam laser used in positive-ion mode over the *m/z* range
858 800–5000, with 4000 laser shots in steps of 800, which were summed to give
859 one spectrum per spot. The Smartbeam™ laser power was set to 50–65%. The
860 Bruker FlexAnalysis software was used to smooth the data (Savitzky-Golay).
861 Following smoothing, all glycan signal intensities assigned a signal-to-noise > 3
862 by the software were selected, and those belonging to the same species (same
863 isotopic envelope) were summed to generate a total signal intensity for each
864 glycan species. Total signal intensities for each glycan were normalized to the

865 total glycan signal within a spectrum, and normalized intensities averaged
866 between spectra collected for the same cell line.

867 For glycan profiling of mouse skin samples, glycans were isolated from
868 E18.5 control and homozygous Gorab^{Null} [47]. The mice were bred with local
869 ethical approval from Landesamt für Gesundheitsschutz und Technische
870 Sicherheit (LaGeTSi), Berlin, Germany (approval number G0213/12). The
871 proteins/glycoproteins were then dialyzed against 50 mM ammonium
872 hydrogen carbonate at 4°C. After lyophilisation, glycoproteins were dissolved in
873 500 µL of 600 mM Tris/HCl pH 8.2 and denatured by guanidine hydrochloride
874 (6M final concentration). The sample was reduced using 1 mg of dithiothreitol
875 and incubated at 50°C for 2h. After addition of 6 mg of iodoacetamide, the
876 sample was incubated at room temperature for 90 min in the dark. The sample
877 was then dialyzed against 50 mM ammonium hydrogen carbonate at 4°C and
878 lyophilized. The reduced carboxyamidomethylated proteins were digested with
879 L-1-tosylamide-2-phenylethylchloromethylketone (TPCK) bovine pancreas
880 trypsin (EC 3.4.21.4, Sigma) with an enzyme-to-substrate ratio of 1:50 (by mass),
881 and the mixture was incubated for 24 h at 37°C in 50 mM ammonium
882 bicarbonate buffer, pH 8.4. The reaction was terminated by boiling for 5 min
883 before lyophilization. PNGase F digestion was carried out in ammonium
884 bicarbonate buffer (50 mM) for 16 h at 37°C. The reaction was terminated by
885 lyophilization and the products were purified on C18-Sep-Pak to separate the *N*-
886 glycans from the de-*N*-glycosylated peptides. After conditioning the C18-Sep-Pak
887 by sequential washing with methanol (5 ml), and 5% acetic acid (2 x 5ml), the
888 sample was loaded onto the Sep-Pak and the N-glycans were eluted with 2 ml of

889 5% acetic acid. N-linked glycans were then permethylated using the sodium
890 hydroxide procedure. MALDI-TOF-MS experiments were carried out on Voyager
891 Elite DE-STR Pro instrument (PersSeptive Biosystem, Framingham, MA, USA)
892 equipped with a pulsed nitrogen laser (337 nm) and a gridless delayed
893 extraction ion source. The spectrometer was operated in positive reflectron
894 mode by delayed extraction with an accelerating voltage of 20 kVand a pulse
895 delay time of 200 ns and a grid voltage of 66%. All the spectra shown represent
896 accumulated spectra obtained by 400–500 laser shots. Sample was prepared by
897 mixing a 1 μL aliquot (5–10 picomoles) with 1 μL of 10 mg/mL 2,5-
898 dihydroxybenzoic acid (in 50% methanol).

899 The assignment of glycan species for both human fibroblast and mouse
900 skin samples was based on accurate *m/z* measurements, precisely matching to
901 theoretical masses of the glycan species measured, taking into account the
902 known ionization of these glycans, and on the basis of the well-accepted
903 biosynthetic route for N-glycans [74,75].
904

905 **Statistical analysis.** Statistical analyses were conducted with use of GraphPad
906 Prism software (GraphPad Software). D'Agostino-Pearson and Shapiro-Wilk
907 tests were used for comparison of the distribution of data with a Gaussian
908 distribution. Depending on the result, an unpaired t-test or Mann-Whitney test
909 was performed. In the case of an unpaired t-test, equality of variances between
910 two groups was tested with an F test. One-way ANOVA with a Dunnett's test was
911 performed for multiple group comparisons and the equality of group variances
912 were examined with a Brown–Forsythe test. Quantification of SialylT-HRP

913 distribution in siRNA-treated HeLa SialylT-HRP cells was performed using a Chi-
914 square test. Statistical significance cut-offs were set as follows: * $p \leq 0.05$, **
915 $p < 0.01$ and *** $p < 0.001$.

916

917 **Data Availability:** The data that support the findings of this study are available
918 from the corresponding author upon request.

919

920 **References**

921 1 Letourneur, F. *et al.* Coatomer is essential for retrieval of dilysine-tagged
922 proteins to the endoplasmic reticulum. *Cell* **79**, 1199-1207 (1994).
923 2 Waters, M. G., Serafini, T. & Rothman, J. E. 'Coatomer': a cytosolic protein
924 complex containing subunits of non-clathrin-coated Golgi transport
925 vesicles. *Nature* **349**, 248-251, doi:10.1038/349248a0 (1991).
926 3 Duden, R., Griffiths, G., Frank, R., Argos, P. & Kreis, T. E. Beta-COP, a 110 kd
927 protein associated with non-clathrin-coated vesicles and the Golgi
928 complex, shows homology to beta-adaptin. *Cell* **64**, 649-665 (1991).
929 4 Orci, L. *et al.* Budding from Golgi membranes requires the coatomer
930 complex of non-clathrin coat proteins. *Nature* **362**, 648-652,
931 doi:10.1038/362648a0 (1993).
932 5 Martinez-Menarguez, J. A. *et al.* Peri-Golgi vesicles contain retrograde but
933 not anterograde proteins consistent with the cisternal progression model
934 of intra-Golgi transport. *J Cell Biol* **155**, 1213-1224,
935 doi:10.1083/jcb.200108029 (2001).
936 6 Lanoix, J. *et al.* Sorting of Golgi resident proteins into different
937 subpopulations of COPI vesicles: a role for ArfGAP1. *J Cell Biol* **155**, 1199-
938 1212, doi:10.1083/jcb.200108017 (2001).
939 7 Orci, L. *et al.* Bidirectional transport by distinct populations of COPI-
940 coated vesicles. *Cell* **90**, 335-349 (1997).
941 8 Pellett, P. A., Dietrich, F., Bewersdorf, J., Rothman, J. E. & Lavieu, G. Inter-
942 Golgi transport mediated by COPI-containing vesicles carrying small
943 cargoes. *Elife* **2**, e01296, doi:10.7554/eLife.01296 (2013).
944 9 Yang, J. S. *et al.* COPI acts in both vesicular and tubular transport. *Nat Cell*
945 *Biol* **13**, 996-1003, doi:10.1038/ncb2273 (2011).
946 10 Oprins, A., Duden, R., Kreis, T. E., Geuze, H. J. & Slot, J. W. Beta-COP
947 localizes mainly to the cis-Golgi side in exocrine pancreas. *J Cell Biol* **121**,
948 49-59 (1993).

949 11 Griffiths, G., Pepperkok, R., Locker, J. K. & Kreis, T. E. Immunocytochemical
950 localization of beta-COP to the ER-Golgi boundary and the TGN. *J Cell Sci*
951 **108 (Pt 8)**, 2839-2856 (1995).
952 12 Serafini, T. *et al.* ADP-ribosylation factor is a subunit of the coat of Golgi-
953 derived COP-coated vesicles: a novel role for a GTP-binding protein. *Cell*
954 **67**, 239-253 (1991).
955 13 Donaldson, J. G., Cassel, D., Kahn, R. A. & Klausner, R. D. ADP-ribosylation
956 factor, a small GTP-binding protein, is required for binding of the
957 coatomer protein beta-COP to Golgi membranes. *Proc Natl Acad Sci U S A*
958 **89**, 6408-6412 (1992).
959 14 Jackson, C. L. & Bouvet, S. Arfs at a glance. *J Cell Sci* **127**, 4103-4109,
960 doi:10.1242/jcs.144899 (2014).
961 15 Beck, R., Rawet, M., Wieland, F. T. & Cassel, D. The COPI system: molecular
962 mechanisms and function. *FEBS Lett* **583**, 2701-2709,
963 doi:10.1016/j.febslet.2009.07.032 (2009).
964 16 Popoff, V., Adolf, F., Brugger, B. & Wieland, F. COPI budding within the
965 Golgi stack. *Cold Spring Harb Perspect Biol* **3**, a005231,
966 doi:10.1101/cshperspect.a005231 (2011).
967 17 Lee, C. & Goldberg, J. Structure of coatomer cage proteins and the
968 relationship among COPI, COPII, and clathrin vesicle coats. *Cell* **142**, 123-
969 132, doi:10.1016/j.cell.2010.05.030 (2010).
970 18 Dodonova, S. O. *et al.* VESICULAR TRANSPORT. A structure of the COPI
971 coat and the role of coat proteins in membrane vesicle assembly. *Science*
972 **349**, 195-198, doi:10.1126/science.aab1121 (2015).
973 19 Bremser, M. *et al.* Coupling of coat assembly and vesicle budding to
974 packaging of putative cargo receptors. *Cell* **96**, 495-506 (1999).
975 20 Berk, D. R., Bentley, D. D., Bayliss, S. J., Lind, A. & Urban, Z. Cutis laxa: a
976 review. *J Am Acad Dermatol* **66**, 842 e841-817,
977 doi:10.1016/j.jaad.2011.01.004 (2012).
978 21 Urban, Z. & Davis, E. C. Cutis laxa: intersection of elastic fiber biogenesis,
979 TGFbeta signaling, the secretory pathway and metabolism. *Matrix Biol* **33**,
980 16-22, doi:10.1016/j.matbio.2013.07.006 (2014).
981 22 Hennies, H. C. *et al.* Gerodermia osteodysplastica is caused by mutations
982 in SCYL1BP1, a Rab-6 interacting golgin. *Nat Genet* **40**, 1410-1412,
983 doi:10.1038/ng.252 (2008).
984 23 Hunter, A. G., Martsolf, J. T., Baker, C. G. & Reed, M. H. Geroderma
985 osteodysplastica. A report of two affected families. *Hum Genet* **40**, 311-
986 324 (1978).
987 24 Lisker, R. *et al.* Gerodermia osteodysplastica hereditaria: report of three
988 affected brothers and literature review. *Am J Med Genet* **3**, 389-395,
989 doi:10.1002/ajmg.1320030410 (1979).
990 25 Egerer, J. *et al.* GORAB Missense Mutations Disrupt RAB6 and ARF5
991 Binding and Golgi Targeting. *J Invest Dermatol* **135**, 2368-2376,
992 doi:10.1038/jid.2015.192 (2015).
993 26 Witkos, T. M. & Lowe, M. The Golgin Family of Coiled-Coil Tethering
994 Proteins. *Front Cell Dev Biol* **3**, 86, doi:10.3389/fcell.2015.00086 (2015).
995 27 Wong, M., Gillingham, A. K. & Munro, S. The golgin coiled-coil proteins
996 capture different types of transport carriers via distinct N-terminal
997 motifs. *BMC Biol* **15**, 3, doi:10.1186/s12915-016-0345-3 (2017).

998 28 Liu, Y. *et al.* SCYL1BP1 modulates neurite outgrowth and regeneration by
999 regulating the Mdm2/p53 pathway. *Mol Biol Cell* **23**, 4506-4514,
1000 doi:10.1091/mbc.E12-05-0362 (2012).
1001 29 Yan, J., Di, Y., Shi, H., Rao, H. & Huo, K. Overexpression of SCYL1-BP1
1002 stabilizes functional p53 by suppressing MDM2-mediated ubiquitination.
1003 *FEBS Lett* **584**, 4319-4324, doi:10.1016/j.febslet.2010.09.019 (2010).
1004 30 Liu, Y. *et al.* Gorab Is Required for Dermal Condensate Cells to Respond to
1005 Hedgehog Signals during Hair Follicle Morphogenesis. *J Invest Dermatol*
1006 **136**, 378-386, doi:10.1016/j.jid.2015.10.067 (2016).
1007 31 Kovacs, L. *et al.* Gorab is a Golgi protein required for structure and
1008 duplication of Drosophila centrioles. *Nat Genet* **50**, 1021-1031,
1009 doi:10.1038/s41588-018-0149-1 (2018).
1010 32 Di, Y. *et al.* Cloning and characterization of a novel gene which encodes a
1011 protein interacting with the mitosis-associated kinase-like protein NTKL.
1012 *J Hum Genet* **48**, 315-321, doi:10.1007/s10038-003-0031-5 (2003).
1013 33 Hamlin, J. N. *et al.* Scyl1 scaffolds class II Arfs to specific subcomplexes of
1014 coatomer through the gamma-COP appendage domain. *J Cell Sci* **127**,
1015 1454-1463, doi:10.1242/jcs.136481 (2014).
1016 34 Burman, J. L. *et al.* Scyl1, mutated in a recessive form of spinocerebellar
1017 neurodegeneration, regulates COPI-mediated retrograde traffic. *J Biol*
1018 *Chem* **283**, 22774-22786, doi:10.1074/jbc.M801869200 (2008).
1019 35 Ma, W. & Goldberg, J. Rules for the recognition of dilysine retrieval motifs
1020 by coatomer. *EMBO J* **32**, 926-937, doi:10.1038/emboj.2013.41 (2013).
1021 36 Gillingham, A. K., Sinka, R., Torres, I. L., Lilley, K. S. & Munro, S. Toward a
1022 comprehensive map of the effectors of rab GTPases. *Dev Cell* **31**, 358-373,
1023 doi:10.1016/j.devcel.2014.10.007 (2014).
1024 37 Popoff, V. *et al.* Several ADP-ribosylation factor (Arf) isoforms support
1025 COPI vesicle formation. *J Biol Chem* **286**, 35634-35642,
1026 doi:10.1074/jbc.M111.261800 (2011).
1027 38 Al-Dosari, M. & Alkuraya, F. S. A novel missense mutation in SCYL1BP1
1028 produces geroderma osteodysplastica phenotype indistinguishable from
1029 that caused by nullimorphic mutations. *Am J Med Genet A* **149A**, 2093-
1030 2098, doi:10.1002/ajmg.a.32996 (2009).
1031 39 Gardeitchik, T. *et al.* Clinical and biochemical features guiding the
1032 diagnostics in neurometabolic cutis laxa. *Eur J Hum Genet* **22**, 888-895,
1033 doi:10.1038/ejhg.2013.154 (2014).
1034 40 Silvius, J. R., Bhagatji, P., Leventis, R. & Terrone, D. K-ras4B and prenylated
1035 proteins lacking "second signals" associate dynamically with cellular
1036 membranes. *Mol Biol Cell* **17**, 192-202, doi:10.1091/mbc.e05-05-0408
1037 (2006).
1038 41 Wong, M. & Munro, S. Membrane trafficking. The specificity of vesicle
1039 traffic to the Golgi is encoded in the golgin coiled-coil proteins. *Science*
1040 **346**, 1256898, doi:10.1126/science.1256898 (2014).
1041 42 Nagaraj, N. *et al.* Deep proteome and transcriptome mapping of a human
1042 cancer cell line. *Mol Syst Biol* **7**, 548, doi:10.1038/msb.2011.81 (2011).
1043 43 Kuliyev, E. *et al.* Overlapping Role of SCYL1 and SCYL3 in Maintaining
1044 Motor Neuron Viability. *J Neurosci* **38**, 2615-2630,
1045 doi:10.1523/JNEUROSCI.2282-17.2018 (2018).

1046 44 Spang, A., Matsuoka, K., Hamamoto, S., Schekman, R. & Orci, L. Coatomer,
1047 Arf1p, and nucleotide are required to bud coat protein complex I-coated
1048 vesicles from large synthetic liposomes. *Proc Natl Acad Sci U S A* **95**,
1049 11199-11204 (1998).
1050 45 Fisher, P. & Ungar, D. Bridging the Gap between Glycosylation and Vesicle
1051 Traffic. *Front Cell Dev Biol* **4**, 15, doi:10.3389/fcell.2016.00015 (2016).
1052 46 Gilormini, P. A. *et al.* A sequential bioorthogonal dual strategy: ManNAl
1053 and SiaNAl as distinct tools to unravel sialic acid metabolic pathways.
1054 *Chem Commun (Camb)* **52**, 2318-2321, doi:10.1039/c5cc08838k (2016).
1055 47 Chan, W. L. *et al.* Impaired proteoglycan glycosylation, elevated TGF-beta
1056 signaling, and abnormal osteoblast differentiation as the basis for bone
1057 fragility in a mouse model for gerodermia osteodysplastica. *PLoS Genet*
1058 **14**, e1007242, doi:10.1371/journal.pgen.1007242 (2018).
1059 48 Jokitalo, E., Cabrera-Poch, N., Warren, G. & Shima, D. T. Golgi clusters and
1060 vesicles mediate mitotic inheritance independently of the endoplasmic
1061 reticulum. *J Cell Biol* **154**, 317-330 (2001).
1062 49 Zolov, S. N. & Lupashin, V. V. Cog3p depletion blocks vesicle-mediated
1063 Golgi retrograde trafficking in HeLa cells. *J Cell Biol* **168**, 747-759,
1064 doi:10.1083/jcb.200412003 (2005).
1065 50 Griffiths, G. & Simons, K. The trans Golgi network: sorting at the exit site
1066 of the Golgi complex. *Science* **234**, 438-443 (1986).
1067 51 Gleeson, P. A., Lock, J. G., Luke, M. R. & Stow, J. L. Domains of the TGN:
1068 coats, tethers and G proteins. *Traffic* **5**, 315-326, doi:10.1111/j.1398-
1069 9219.2004.00182.x (2004).
1070 52 Burman, J. L., Hamlin, J. N. & McPherson, P. S. Scyl1 regulates Golgi
1071 morphology. *PLoS One* **5**, e9537, doi:10.1371/journal.pone.0009537
1072 (2010).
1073 53 Duwel, M. & Ungewickell, E. J. Clathrin-dependent association of CVAK104
1074 with endosomes and the trans-Golgi network. *Mol Biol Cell* **17**, 4513-
1075 4525, doi:10.1091/mbc.e06-05-0390 (2006).
1076 54 Sullivan, A., Uff, C. R., Isacke, C. M. & Thorne, R. F. PACE-1, a novel protein
1077 that interacts with the C-terminal domain of ezrin. *Exp Cell Res* **284**, 224-
1078 238 (2003).
1079 55 Borner, G. H. *et al.* CVAK104 is a novel regulator of clathrin-mediated
1080 SNARE sorting. *Traffic* **8**, 893-903, doi:10.1111/j.1600-
1081 0854.2007.00576.x (2007).
1082 56 Schmidt, W. M. *et al.* Mutation in the Scyl1 gene encoding amino-terminal
1083 kinase-like protein causes a recessive form of spinocerebellar
1084 neurodegeneration. *EMBO Rep* **8**, 691-697,
1085 doi:10.1038/sj.embor.7401001 (2007).
1086 57 Schmidt, W. M. *et al.* Disruptive SCYL1 Mutations Underlie a Syndrome
1087 Characterized by Recurrent Episodes of Liver Failure, Peripheral
1088 Neuropathy, Cerebellar Atrophy, and Ataxia. *Am J Hum Genet* **97**, 855-861,
1089 doi:10.1016/j.ajhg.2015.10.011 (2015).
1090 58 Lenz, D. *et al.* SCYL1 variants cause a syndrome with low gamma-
1091 glutamyl-transferase cholestasis, acute liver failure, and
1092 neurodegeneration (CALFAN). *Genet Med*, doi:10.1038/gim.2017.260
1093 (2018).

1094 59 Freeze, H. H. Genetic defects in the human glycome. *Nat Rev Genet* **7**, 537-
1095 551, doi:10.1038/nrg1894 (2006).
1096 60 Willett, R., Ungar, D. & Lupashin, V. The Golgi puppet master: COG
1097 complex at center stage of membrane trafficking interactions. *Histochem*
1098 *Cell Biol* **140**, 271-283, doi:10.1007/s00418-013-1117-6 (2013).
1099 61 Kornak, U. *et al.* Impaired glycosylation and cutis laxa caused by
1100 mutations in the vesicular H+-ATPase subunit ATP6V0A2. *Nat Genet* **40**,
1101 32-34, doi:10.1038/ng.2007.45 (2008).
1102 62 Hucthagowder, V. *et al.* Loss-of-function mutations in ATP6V0A2 impair
1103 vesicular trafficking, tropoelastin secretion and cell survival. *Hum Mol*
1104 *Genet* **18**, 2149-2165, doi:10.1093/hmg/ddp148 (2009).
1105 63 Seidler, D. G. The galactosaminoglycan-containing decorin and its impact
1106 on diseases. *Curr Opin Struct Biol* **22**, 578-582,
1107 doi:10.1016/j.sbi.2012.07.012 (2012).
1108 64 Seidler, D. G. *et al.* Defective glycosylation of decorin and biglycan, altered
1109 collagen structure, and abnormal phenotype of the skin fibroblasts of an
1110 Ehlers-Danlos syndrome patient carrying the novel Arg270Cys
1111 substitution in galactosyltransferase I (beta4GalT-7). *J Mol Med (Berl)* **84**,
1112 583-594, doi:10.1007/s00109-006-0046-4 (2006).
1113 65 Maccarana, M. *et al.* Dermatan sulfate epimerase 1-deficient mice have
1114 reduced content and changed distribution of iduronic acids in dermatan
1115 sulfate and an altered collagen structure in skin. *Mol Cell Biol* **29**, 5517-
1116 5528, doi:10.1128/MCB.00430-09 (2009).
1117 66 Miyake, N. *et al.* Loss-of-function mutations of CHST14 in a new type of
1118 Ehlers-Danlos syndrome. *Hum Mutat* **31**, 966-974,
1119 doi:10.1002/humu.21300 (2010).
1120 67 Malfait, F. *et al.* Defective initiation of glycosaminoglycan synthesis due to
1121 B3GALT6 mutations causes a pleiotropic Ehlers-Danlos-syndrome-like
1122 connective tissue disorder. *Am J Hum Genet* **92**, 935-945,
1123 doi:10.1016/j.ajhg.2013.04.016 (2013).
1124 68 Kitazawa, D., Yamaguchi, M., Mori, H. & Inoue, Y. H. COPI-mediated
1125 membrane trafficking is required for cytokinesis in Drosophila male
1126 meiotic divisions. *J Cell Sci* **125**, 3649-3660, doi:10.1242/jcs.103317
1127 (2012).
1128 69 Pevzner, I. *et al.* Distinct role of subcomplexes of the COPI coat in the
1129 regulation of ArfGAP2 activity. *Traffic* **13**, 849-856, doi:10.1111/j.1600-
1130 0854.2012.01349.x (2012).
1131 70 Hyvola, N. *et al.* Membrane targeting and activation of the Lowe syndrome
1132 protein OCRL1 by rab GTPases. *EMBO J* **25**, 3750-3761,
1133 doi:10.1038/sj.emboj.7601274 (2006).
1134 71 Diao, A., Frost, L., Morohashi, Y. & Lowe, M. Coordination of golgin
1135 tethering and SNARE assembly: GM130 binds syntaxin 5 in a p115-
1136 regulated manner. *J Biol Chem* **283**, 6957-6967,
1137 doi:10.1074/jbc.M708401200 (2008).
1138 72 Diao, A., Rahman, D., Pappin, D. J., Lucocq, J. & Lowe, M. The coiled-coil
1139 membrane protein golgin-84 is a novel rab effector required for Golgi
1140 ribbon formation. *J Cell Biol* **160**, 201-212, doi:10.1083/jcb.200207045
1141 (2003).

1142 73 Willett, R. A., Pokrovskaya, I. D. & Lupashin, V. V. Fluorescent microscopy
1143 as a tool to elucidate dysfunction and mislocalization of Golgi
1144 glycosyltransferases in COG complex depleted mammalian cells. *Methods*
1145 *Mol Biol* **1022**, 61-72, doi:10.1007/978-1-62703-465-4_6 (2013).
1146 74 Abdul Rahman, S. *et al.* Filter-aided N-glycan separation (FANGS): a
1147 convenient sample preparation method for mass spectrometric N-glycan
1148 profiling. *J Proteome Res* **13**, 1167-1176, doi:10.1021/pr401043r (2014).
1149 75 Morelle, W. & Michalski, J. C. Analysis of protein glycosylation by mass
1150 spectrometry. *Nat Protoc* **2**, 1585-1602, doi:10.1038/nprot.2007.227
1151 (2007).

1152

1153 **Acknowledgements**

1154 TMW was supported by a PhD studentship from the Wellcome Trust
1155 (096601/Z/11/Z) and ML by an MRC research grant (MR/N000366/1). We
1156 thank the Wellcome Trust for equipment grant support to the EM Facility. The
1157 Bioimaging Facility microscopes used in this study were purchased with grants
1158 from BBSRC, Wellcome and the University of Manchester Strategic Fund. Special
1159 thanks go to Peter March for his help with the light microscopy and Mike Jackson
1160 from the Flow Cytometry Core Facility for his help and advice. The York Centre of
1161 Excellence in Mass Spectrometry was created thanks to a major capital
1162 investment through Science City York, supported by Yorkshire Forward with
1163 funds from the Northern Way Initiative. UK received funding from the EU (E-
1164 Rare project EURO-CDG-2) and from the German Federal Ministry of Education
1165 and Research (BMBF) (DIMEOs (1EC1402B)). We give thanks to various
1166 colleagues for generously providing reagents as indicated in the Methods
1167 section, and thank Prof. Philip Woodman (University of Manchester) for
1168 comments on the manuscript.

1169

1170 **Author Contributions:** ML managed the project and together with TMW
1171 conceptualized the experiments. TMW performed all the experiments apart
1172 those described below. TMW and ML analyzed the data. TMW prepared the
1173 figures for the manuscript. ML wrote the manuscript with input from all co-
1174 authors. MT helped conceive the project and provided patient fibroblasts. WLC and
1175 UK generated the GORAB knockout mouse and prepared tissues from it. MJ and
1176 EJ generated and analyzed the immuno-EM and fibroblast EM data. AAM
1177 performed the EM analysis of the HRP-ST cells. EP, JTO and DU generated and
1178 analyzed the glycomics data for fibroblast cells. WM performed the glycan
1179 analysis of the GORAB knockout mouse samples. APM helped perform the
1180 surface plasmon resonance experiments. CB and YG made and provided
1181 expertise in the use of alkyne-tagged sialic acid. MR and FTW provided assistance
1182 with the liposome experiments.

1183

1184 **Competing Interests:** The authors declare no competing interests.

1185

1186 **Figure Legends**

1187 **Figure 1. GORAB interacts directly with the NTK domain of Scyl1. A.** Yeast
1188 two-hybrid assay between GORAB and Scyl1 constructs. Prey (AD-GORAB or AD-
1189 Scyl1) and bait (BD-Scyl1 or BD-GORAB) constructs were co-transformed into
1190 yeast and grown on double-drop out (DDO) medium to verify expression of both
1191 proteins in transformants and on selective quadruple drop-out (QDO) medium to
1192 examine protein-protein interactions. Constructs containing AD and BD only

1193 were used as negative controls. **B.** Pull-down assays with recombinant GORAB.
1194 Top panel: pull-down using bacterially expressed GST and GST-GORAB as bait
1195 and sHeLa cell lysate. Bottom panel: pull-down using GST, GST-tagged GORAB or
1196 Syntaxin 1 as bait and rat liver Golgi (RLG) membrane extract. Samples were
1197 blotted with the indicated antibodies. I, input (5%), U, unbound fraction (5%), B,
1198 bound fraction (50%). **C.** Pull-down assay using purified GST-Syntaxin 1 or GST-
1199 GORAB as bait and MBP-tagged Scyl1. Samples were subjected to SDS-PAGE and
1200 analyzed by Coomassie Blue staining. GST-tagged proteins are marked with an
1201 asterisk. BSA used as a carrier protein is marked with a circle. The faint bands
1202 running under MBP-Scyl1 correspond to likely degradation products or bacterial
1203 contaminants. **D.** Mapping the binding site for Scyl1 on GORAB. Left, pull-down
1204 assay using purified GST-tagged GORAB fragments as bait and MBP-tagged Scyl1.
1205 Samples were subjected to SDS-PAGE and Coomassie Blue staining. GST-tagged
1206 proteins are marked with an asterisk. Right, schematic diagram of GST-tagged
1207 GORAB truncation constructs. **E.** Mapping the interaction site for GORAB on
1208 Scyl1. Left, cell lysates obtained from cells transiently expressing GFP-tagged
1209 Scyl1 constructs were used for a pull-down assay with GST or GST-GORAB as bait
1210 and analyzed by Western blotting. GST-tagged bait proteins and GFP-tagged
1211 proteins in inputs are marked with black or red asterisks respectively. Right, a
1212 schematic diagram of GFP-tagged Scyl1 truncation constructs. CC – coiled-coil
1213 region, COPI – COPI binding motif.

1214

1215 **Figure 2. GORAB co-localizes with Scyl1 and COPI in discrete domains at the**
1216 ***trans*-Golgi. A.** Analysis of GORAB localization at the Golgi. Human dermal

1217 fibroblasts were fixed and labeled with antibodies to GORAB, GM130 and TGN46.
1218 Scale bar, 10 μm. The linescan is representative of data from n = 20 cells. **B.**
1219 Analysis of GFP-GORAB localization in stably transfected HeLaM cells (top) and
1220 in HeLaM cells transfected with GORAB siRNA (bottom). Cells were fixed and
1221 labeled with antibodies to GORAB (bottom row only) and TGN46. Scale bar, 10
1222 μm. **C.** GORAB Golgi localization using STED microscopy. Human dermal
1223 fibroblasts were fixed and labeled with antibodies against GORAB and TGN46.
1224 Scale bar, 1 μm. **D** and **E.** Representative EM micrographs depict localization of
1225 GORAB in HeLa cells (D) and human dermal fibroblasts (E). G, Golgi. Scale bars,
1226 500 nm. **F.** Co-localization analysis of GORAB, Scyl1 and β'-COP using STED
1227 microscopy. Human dermal fibroblasts were fixed and labeled with antibodies
1228 against Scyl1, GORAB and β'-COP. Scale bar, 200 nm. Yellow arrowheads mark
1229 GORAB puncta co-localizing both with Scyl1 and β'-COP, magenta arrowheads
1230 mark GORAB puncta co-localizing with Scyl1 only and cyan arrowheads mark
1231 Scyl1 puncta co-localizing with ⍰'-COP but devoid of GORAB. **G. C**o-localization
1232 analysis of GORAB and Rab6 using STED microscopy. Human dermal fibroblasts
1233 were fixed and labeled with antibodies against GORAB and Rab6. Top, scale bar,
1234 5 μm, bottom, scale bar, 200 nm.

1235

1236 **Figure 3. GORAB domains are stable entities. A.** Fluorescence recovery after
1237 photobleaching. Left, FRAP recovery curves for GFP-GalNAc-T2, GFP-GORAB and
1238 GFP-Scy1. Means with SEM for GFP-GalNAc-T2 (n = 27 cells), GFP-GORAB (n = 28
1239 cells) and GFP-Scyl1 (n = 18 cells). Dotted lines mark points of half-time
1240 recoveries. Right, representative HeLa GFP-GalNAc-T2, HeLaM GFP-GORAB and

1241 HeLaM GFP-Scyl1 cells at pre-bleached and selected post-bleached states.
1242 Bleached region of interests are marked with yellow boxes. Scale bar, 10 μm.
1243 **B.** Localization of GORAB in Scyl1-depleted cells. HeLa cells transfected with
1244 control or Scyl1 siRNA were fixed and labeled with antibodies to Scyl1 and
1245 GORAB. Scale bars, 10 μm and 1 μm. GORAB domains are marked with yellow
1246 arrowheads. **C.** Localization of GORAB in BFA-treated cells. HeLa cells were
1247 exposed to 5 μg/mL BFA for 7 min prior to fixation and labeling with antibodies
1248 to Scyl1 and GORAB. Scale bars, 10 μm and 1 μm. GORAB domains are marked
1249 with yellow arrowheads.

1250

1251 **Figure 4. Effect of pathogenic missense mutations upon GORAB behavior.**
1252 **A.** Location of known missense and single base deletion GORAB mutations in GO
1253 patients. Coiled-coil domains are depicted as orange rectangles. **B.** Interaction of
1254 GORAB variants with GST-tagged bait proteins, as indicated, using cell lysates
1255 from RPE-1 cells expressing the indicated GFP-tagged GORAB variants. Inputs
1256 (5%) and bound fractions (50%) were blotted for GFP. **C.** Surface plasmon
1257 resonance analysis of GORAB-Scyl1 binding. Top, experimental setup with a GLH
1258 sensor chip, cross-linked anti-MBP antibody, MBP-Scyl1 as bound ligand and
1259 GST-GORAB variants as analyte. Bottom, binding of GST-GORAB variants at 30
1260 nM concentration for 120 s followed by 600 s disassociation. Similar results
1261 were obtained in three separate experiments. **D.** Golgi localization of GFP-tagged
1262 GORAB variants using STED microscopy. RPE-1 cells were fixed and labeled with
1263 TGN46 antibodies. Scale bar, 5 μm. **E.** COPI subcellular localization in HeLaM
1264 cells transfected with GFP or GFP-GORAB and incubated for 10 min with 5

1265 μg/mL BFA. Cells were labeled with antibodies to β'-COP and GM130. Scale bar,
1266 10 μm. Dotted line marks the nucleus. **F.** Quantification of COPI retention in the
1267 Golgi region from panel E. Error bars represent mean ± SD, n=100 cells in each of
1268 3 independent experiments, * $p \leq 0.05$ and *** $p < 0.001$, unpaired t-test. **G.** COPI
1269 subcellular localization in HeLaM cells transfected with GFP or GFP-Scyl1 fixed
1270 10 min after incubation with 5 μg/mL BFA. Cells were labeled with antibodies to
1271 β'-COP and GM130. Scale bar, 10 μm. Dotted line marks the nucleus.
1272 **H.** Quantification of COPI retention in the Golgi region from panel G. Error bars
1273 represent mean ± SD, n=100 cells in each of 3 independent experiments, ***
1274 $p < 0.001$, unpaired t-test. **I.** Co-localization between GFP-Scyl1, β'-COP and
1275 GORAB in HeLaM cells fixed 10 min after incubation with 5 μg/mL BFA. Cells
1276 were labeled with antibodies to GORAB and β'-COP. Scale bar, 10 μm. Dotted line
1277 marks the cell boundary. The white line indicates the pixels used for the RGB
1278 fluorescence intensity profile plot on the right, which is representative of data
1279 from n = 20 cells.

1280

1281 **Figure 5. GORAB, via Scyl1, is sufficient to recruit COPI to membranes. A.** A
1282 schematic diagram depicting the mitochondrial relocation assay where the
1283 addition of rapamycin induces mitochondrial relocation of FKBP-tagged GORAB,
1284 allowing for recruitment of associated factors to this compartment. **B.** Relocation
1285 of GORAB-mycFKBP and co-expressed GFP-Scyl1 to mitochondria. HeLaM cells
1286 co-transfected with mito-FRB and GORABK190del-mycFKBP constructs were
1287 pretreated with 2.5 μg/mL nocodazole for 2 h and further incubated with 1 μM
1288 rapamycin or DMSO for 3 h prior to fixation. Cells were labeled with antibodies

1289 to myc and mtHsp70. **C.** Relocation of endogenous Scyl1 to mitochondria by
1290 GORAB-mycFKBP. HeLaM cells co-transfected with mito-FRB and GORAB-
1291 mycFKBP and treated as described in B and labeled with antibodies to
1292 endogenous Scyl1 and the Golgi marker β4GalT1. **D**. Relocation of COPI to
1293 mitochondria by GORAB-mycFKBP. HeLaM cells co-transfected with mito-FRB,
1294 GORABK190del-mycFKBP and GFP-Scyl1 were treated as in B, and additionally
1295 with 5 μg/mL BFA for 15 min (lower panel only). Cells were labeled with
1296 antibodies to β'-COP and myc. In panels B-D, scale bars are 10 μm and white lines
1297 indicate the pixels used for the RGB fluorescence intensity profile plots shown on
1298 the right, which are representative of data from n = 20 cells.

1299

1300 **Figure 6. Scyl1-dependent recruitment of COPI to artificial membranes.**
1301 **A.** Liposome recruitment assay with purified MBP-Scyl1, myr-Arf1 and
1302 recombinant coatomer. Inputs (2%) and membrane bound fractions (40%) were
1303 subjected to SDS-PAGE and blotted for MBP, ε-COP and Arf1. **B.** Liposome
1304 recruitment assay with purified MBP-IPIP27A (as negative control), MBP-Scyl1
1305 and myr-Arf1 and recombinant coatomer. Inputs (2%) and membrane bound
1306 fractions (40%) were subjected to SDS-PAGE and blotted for MBP, δ-COP, ε-COP
1307 and Arf1. **C.** Quantification of recruitment of Arf1 and coatomer (δ-COP, ε-COP)
1308 to liposomes in the presence of MBP-IPIP27A and MBP-Scyl1. Error bars
1309 represent mean ± SD, n=6 independent experiments, ** $p<0.01$, *** $p<0.001$,
1310 unpaired t-test.

1311

1312 **Figure 7. Loss of GORAB causes defective terminal N-glycosylation of**
1313 **proteins. A.** *N*-glycome analysis of WT and GO fibroblasts. Quantification of
1314 relative intensities of MALDI-TOF-MS signals for *N*-glycan species detected in
1315 lysates from wild-type (N=3 cell lines) and GO fibroblasts (N=4 cell lines). Error
1316 bars represent the mean ± SEM from 4 independent experiments, * $p<0.05$,
1317 unpaired t-test. GlcNAc, N-acetylglucosamine, NeuAc, N-acetylneuraminic acid,
1318 NeuGc, N-glycolylneuraminic acid. Yellow shading indicates differences between
1319 WT and GO fibroblasts. **B.** Analysis of sialylated plasma membrane proteins in
1320 WT and GO fibroblasts using MAL and SNA lectins. Top, glycan chains recognized
1321 by the lectins. Bottom, non-permeabilized fibroblasts stained with FITC-
1322 conjugated lectins. Scale bar, 10 μm. **C.** Quantification of fluorescence intensities
1323 from panel B (150 cells analyzed per cell line in each of 3 independent
1324 experiments, min to max box and whisker plot, ** $p<0.01$, Mann-Whitney *U* test.
1325 **D.** Representative flow cytometry histogram of WT and GO fibroblasts (N=3 cell
1326 lines) stained with FITC-conjugated MAL and SNA lectins. **E.** Analysis of
1327 metabolic labeling of WT and GO fibroblasts with alkynyl-tagged sialic acid
1328 precursor ManNAl. Co-cultured WT and GO cells were incubated with ManNAI
1329 for 10 h, fixed and labeled with antibodies to GORAB and TGN46. Scale bar, 10
1330 μm. **F.** Quantification of ManNAI labeling assessed as fluorescence intensity
1331 against that of a Golgi marker, with 300 cells analyzed per cell line in 3
1332 independent experiments, min to max box and whisker plot, *** $p<0.001$, Mann-
1333 Whitney *U* test. **G.** *N*-glycome analysis of control and *Gorab*^{Null} mouse skin tissue.
1334 Symbols representing monosaccharide residues are as in A. Yellow shading
1335 indicates N-glycans different between control and *Gorab*^{Null} samples. **H** and **I.**
1336 Left, lectin blot analysis of skin lysates of control and *Gorab*^{Null} E18.5 embryos

1337 with E-PHA (H) or SNA lectin (I). Right, quantification of E-PHA (H) or SNA (I)
1338 levels. Error bars represent the mean+SD, n=4 independent experiments, *
1339 p<0.05, ** p<0.01, unpaired t-test. In panels A and G, the glycan colored symbols
1340 are drawn according to the Symbol Nomenclature For Glycans convention. The
1341 structures shown are those most probable for compositions determined from
1342 accurate *m/z* measurements on the basis of the well-accepted biosynthetic route
1343 for *N*-glycans. Glycan assignments and accompanying masses in panel G are
1344 shown in Supplementary Table 1.

1345

1346 **Figure 8. Loss of GORAB alters SialylT localization and Golgi ultrastructure.**
1347 **A.** Knock-down of GORAB, Scyl1 and Cog3 proteins in HeLa SialylT-HRP cells.
1348 SiRNA transfected HeLa SialylT-HRP cells were lysed, subjected to SDS-PAGE and
1349 blotted for GORAB, Scyl1, Cog3 and GAPDH. **B.** Representative EM micrographs
1350 depict localization of SialylT-HRP, detected using the DAB reaction to generate
1351 electron dense product, in HeLa SialylT-HRP cells transfected with the indicated
1352 siRNAs. Scale bar, 500 nm. **C.** Quantification of SialylT-HRP distribution in siRNA-
1353 treated HeLa SialylT-HRP cells (n=22 cells per condition, *** p<0.001, Chi-square
1354 test). **D.** Representative conventional thin section EM micrographs of Golgi
1355 ultrastructure in WT (n=4 cell lines) and GO fibroblasts (n=3 cell lines). Enlarged
1356 profiles within Golgi cisternae are marked with a red asterisk. Scale bar, 500 nm.
1357 **E.** Quantification of cells with dilated cisternae. Error bars represent mean ± SD,
1358 n = 25 cells per cell line , ** p<0.01, Chi-square test. **F.** Proposed model for
1359 GORAB function in COPI-mediated trafficking at the *trans*-Golgi. (I) GORAB
1360 oligomers are stably associated with the *trans*-Golgi membrane, forming discrete

1361 domains, while GTP-loading of Arf GTPase leads to its association with the
1362 membrane. (II) Membrane-associated GORAB oligomers recruit Scyl1 and locally
1363 concentrate GTP-bound Arf in the domains, facilitating the efficient recruitment
1364 of coatomer by coincident detection. (III) Coatomer accumulates in the domains
1365 and begins to self-assemble. (IV) Coatomer assembly leads to cargo
1366 incorporation into a newly forming COPI vesicle. (V) GORAB may stabilize
1367 coatomer assembly by remaining associated with the bud neck during vesicle
1368 formation. (V) The completed COPI vesicle detaches from the membrane
1369 alongside Scyl1, while GORAB stays at the membrane ready to initiate the
1370 biogenesis of a new COPI vesicle.

1371

1372

1373

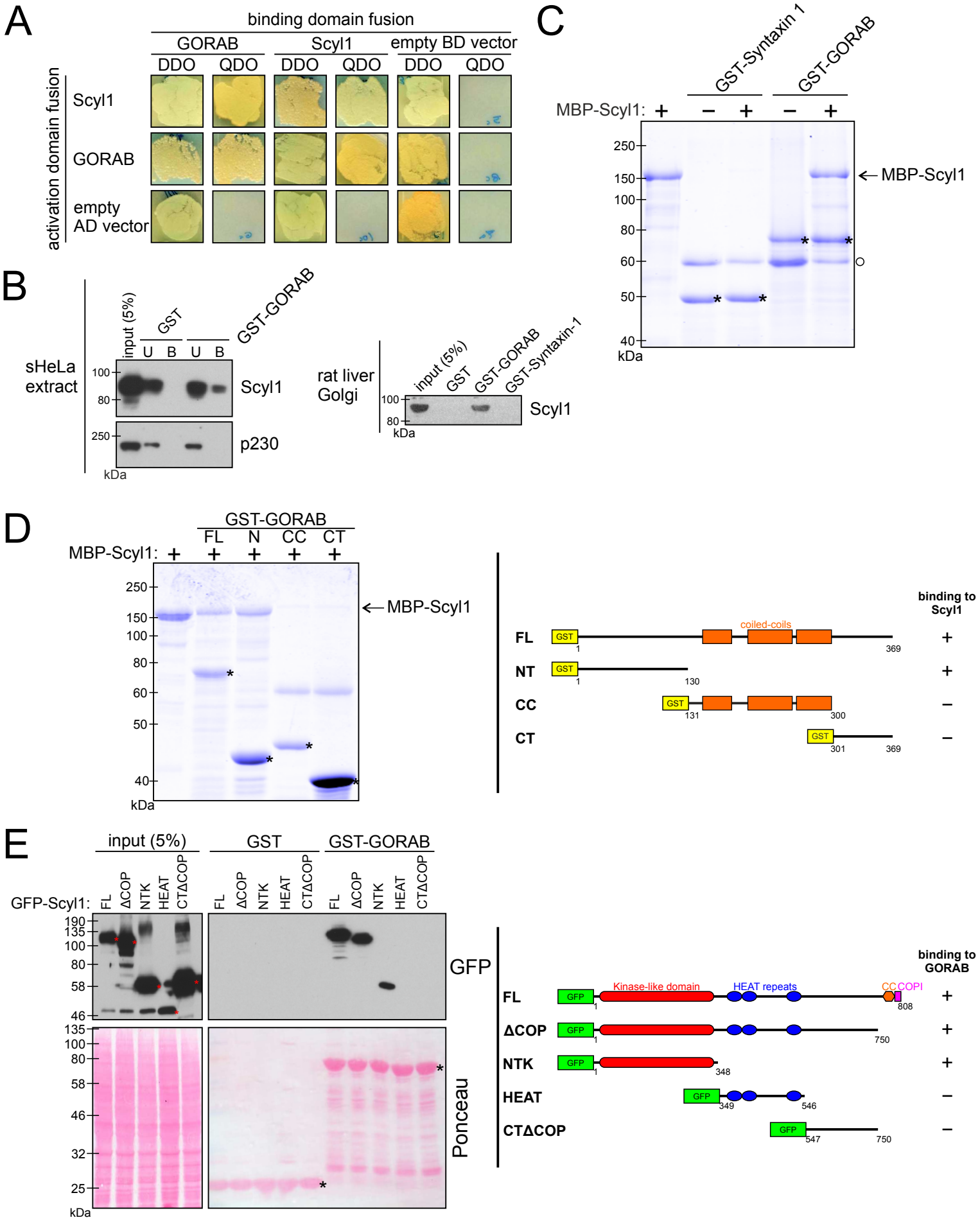
A
binding domain fusion
GORAB
Scyl1
empty BD vector
DDO
QDO
activation domain fusion
Scyl1
GORAB
empty AD vector
B
sHeLa extract
input (5%)
GST
GST-GORAB
U B U B
100
80
Scyl1
250
p230
kDa
rat liver Golgi
input (5%)
GST
GST-GORAB
GST-Syntaxin-1
100
80
Scyl1
kDa
C
GST-Syntaxin 1
GST-GORAB
MBP-Scyl1: + − + − +
250
150
100
80
60
50
40
kDa
MBP-Scyl1
D
GST-GORAB
FL N CC CT
MBP-Scyl1: + + + + +
250
150
100
80
60
50
40
kDa
MBP-Scyl1
binding to Scyl1
FL
GST
coiled-coils
1
369
+
NT
GST
1
130
+
CC
GST
131
300
−
CT
GST
301
369
−
E
input (5%)
GST
GST-GORAB
GFP-Scyl1:
FL
ΔCOP
NTK
HEAT
CTΔCOP
190
135
100
80
58
46
GFP
135
100
80
58
46
32
25
kDa
Ponceau
binding to GORAB
FL
GFP
Kinase-like domain
HEAT repeats
CC COPI
1
808
+
ΔCOP
GFP
1
750
+
NTK
GFP
1
348
+
HEAT
GFP
349
546
−
CTΔCOP
GFP
547
750
−

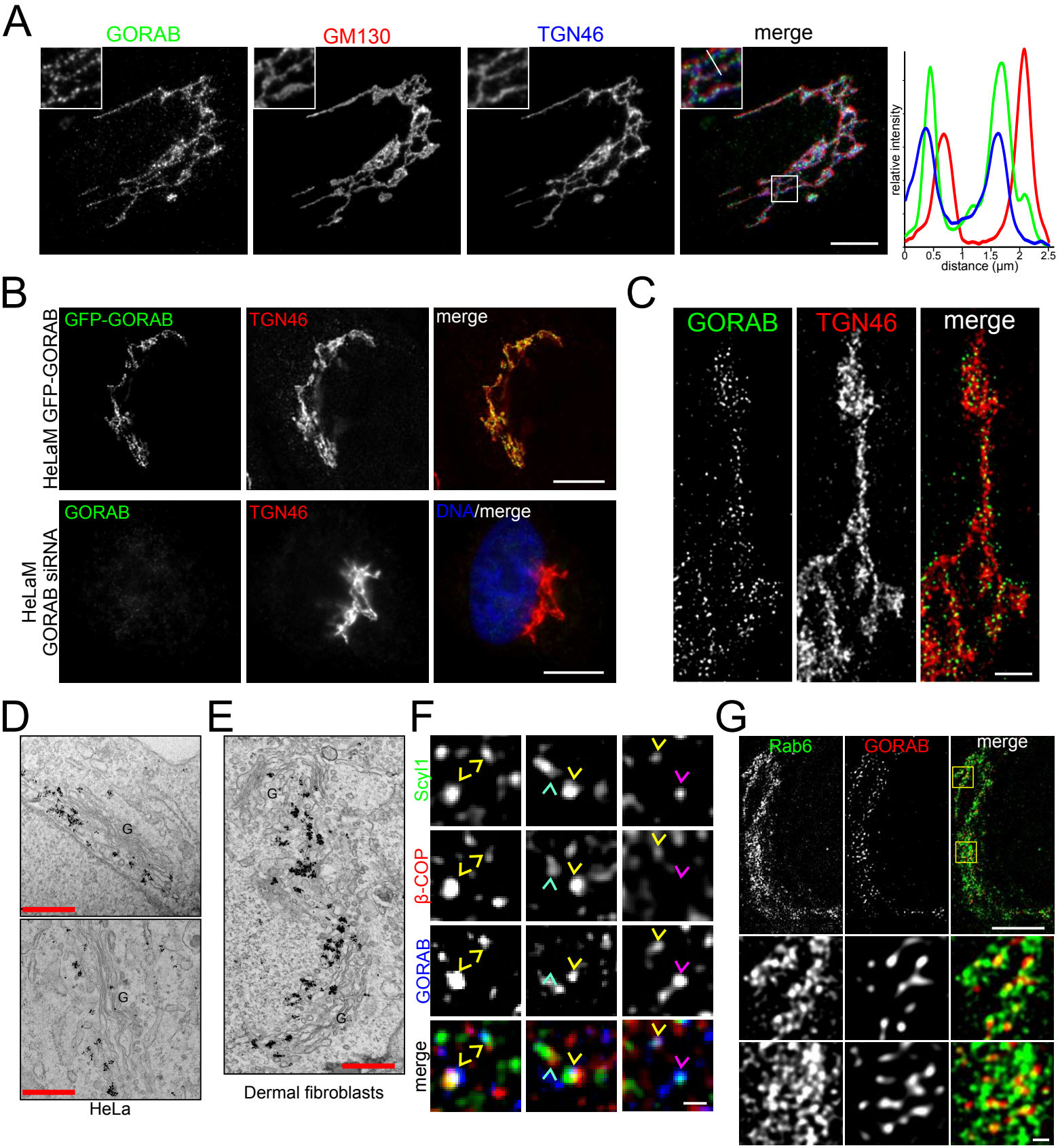
A
GORAB
GM130
TGN46
merge
relative intensity
distance (µm)
0
0.5
1
1.5
2
2.5
B
HeLaM GFP-GORAB
GFP-GORAB
TGN46
merge
HeLaM GORAB siRNA
GORAB
TGN46
DNA/merge
C
GORAB
TGN46
merge
D
G
HeLa
E
G
Dermal fibroblasts
F
Scyl1
β-COP
GORAB
merge
G
Rab6
GORAB
merge

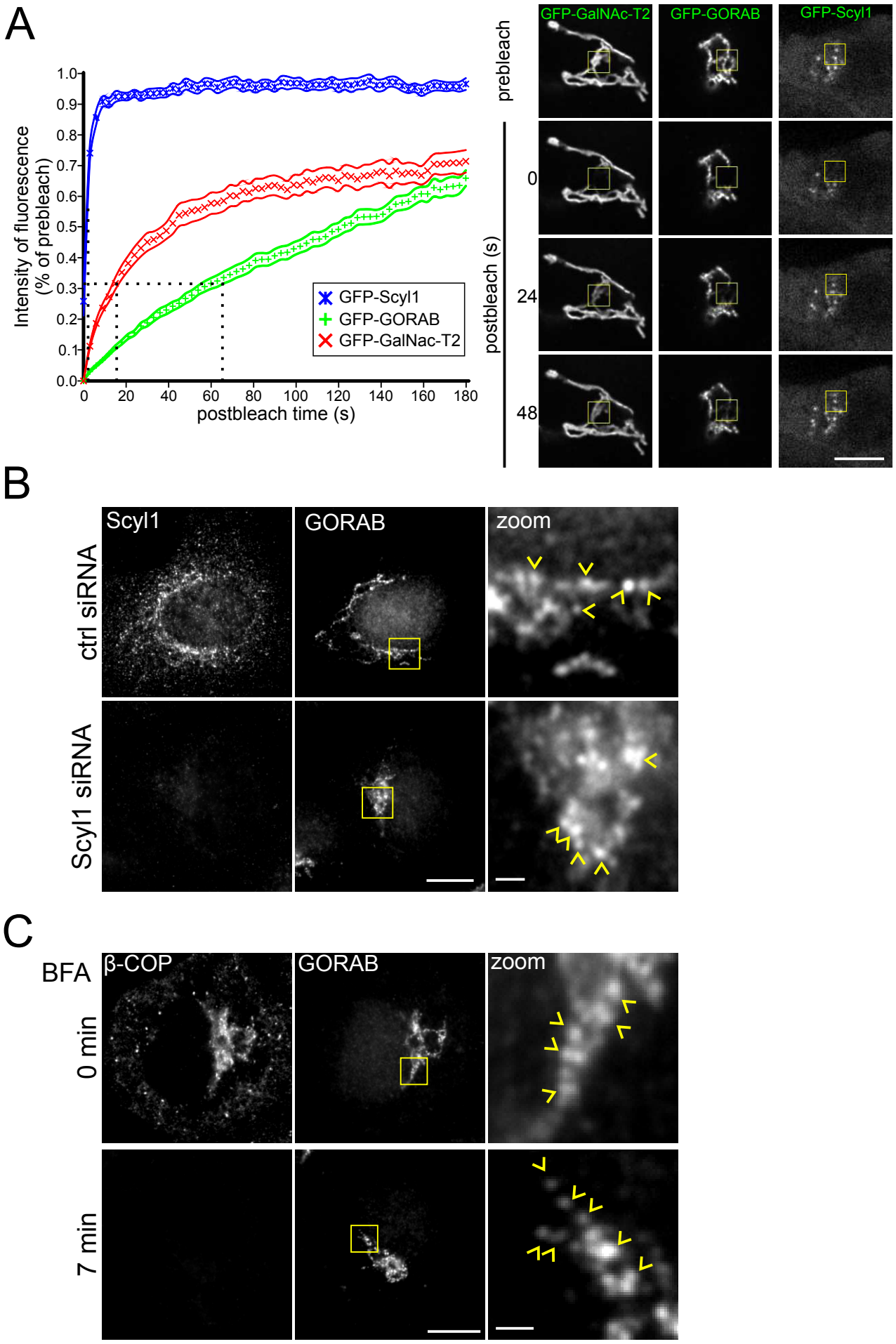
A
Intensity of fluorescence (% of prebleach)
postbleach time (s)
GFP-Scyl1
GFP-GORAB
GFP-GalNac-T2
GFP-GalNAc-T2
GFP-GORAB
GFP-Scyl1
prebleach
postbleach (s)
0
24
48
B
Scyl1
GORAB
zoom
ctrl siRNA
Scyl1 siRNA
C
BFA
β-COP
GORAB
zoom
0 min
7 min

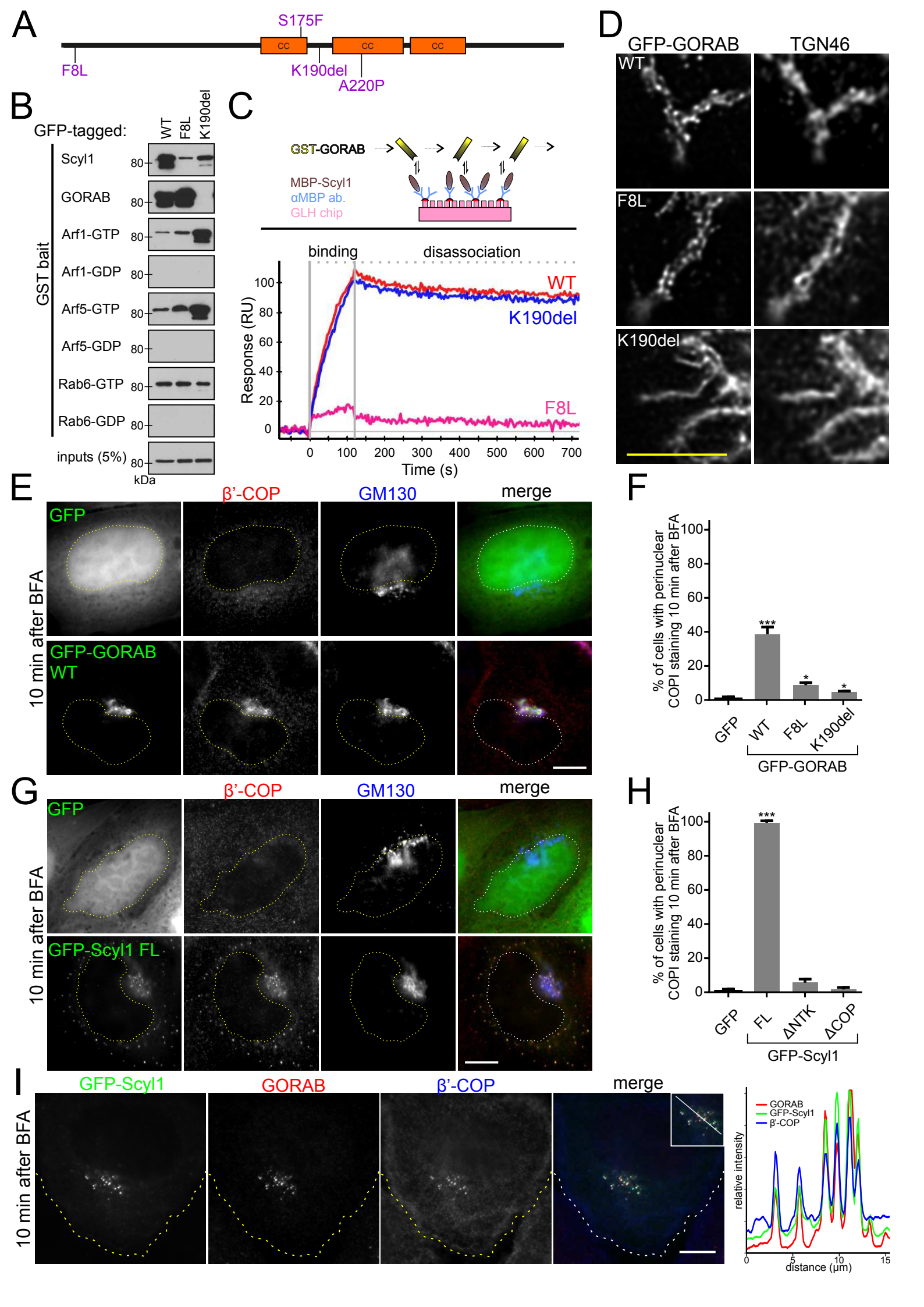
A
S175F
CC
CC
CC
F8L
K190del
A220P
B
GFP-tagged:
WT
F8L
K190del
GST bait
Scyl1
GORAB
Arf1-GTP
Arf1-GDP
Arf5-GTP
Arf5-GDP
Rab6-GTP
Rab6-GDP
inputs (5%)
80
kDa
C
GST-GORAB
MBP-Scyl1
αMBP ab.
GLH chip
binding
disassociation
Response (RU)
WT
K190del
F8L
Time (s)
D
GFP-GORAB
TGN46
WT
F8L
K190del
E
β'-COP
GM130
merge
GFP
GFP-GORAB WT
10 min after BFA
F
% of cells with perinuclear COPI staining 10 min after BFA
GFP
WT
F8L
K190del
GFP-GORAB
G
GFP-Scyl1 FL
H
GFP
FL
ΔNTK
ΔCOP
GFP-Scyl1
I
GFP-Scyl1
GORAB
β'-COP
merge
relative intensity
distance (μm)

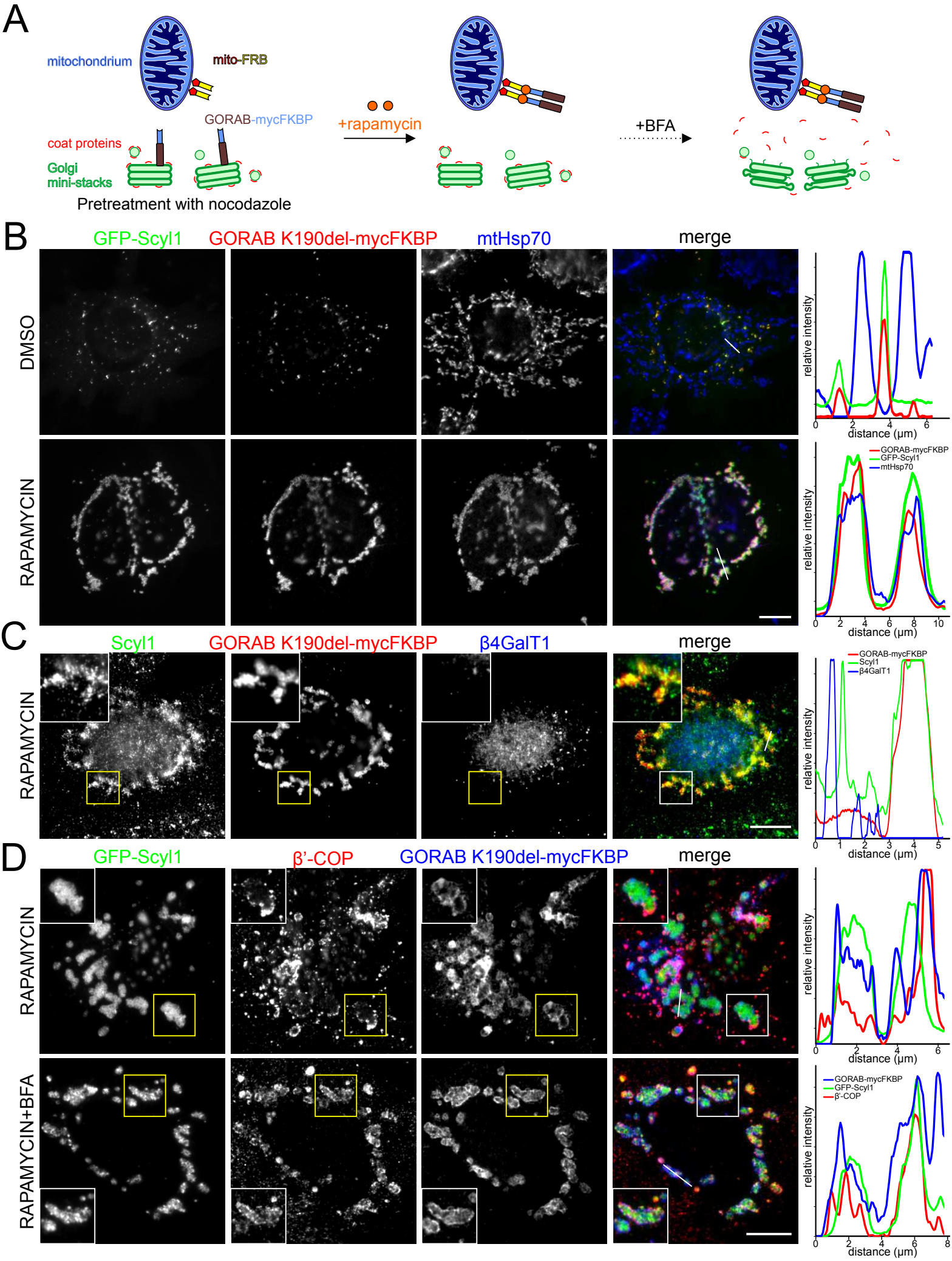
A
mitochondrium
mito-FRB
GORAB-mycFKBP
coat proteins
Golgi mini-stacks
+rapamycin
+BFA
Pretreatment with nocodazole
B
GFP-Scyl1
GORAB K190del-mycFKBP
mtHsp70
merge
DMSO
RAPAMYCIN
relative intensity
distance (µm)
GORAB-mycFKBP
GFP-Scyl1
mtHsp70
C
Scyl1
GORAB K190del-mycFKBP
β4GalT1
merge
RAPAMYCIN
GORAB-mycFKBP
Scyl1
β4GalT1
D
GFP-Scyl1
β'-COP
GORAB K190del-mycFKBP
merge
RAPAMYCIN
RAPAMYCIN+BFA
GORAB-mycFKBP
GFP-Scyl1
β'-COP

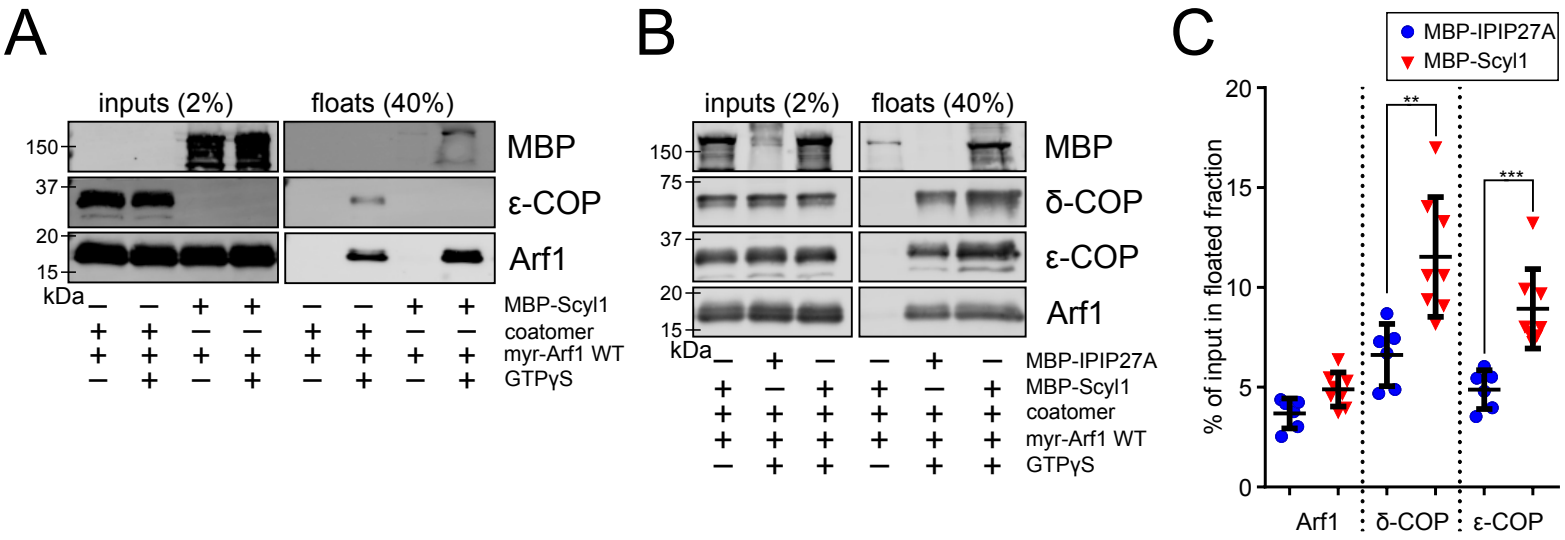
A
inputs (2%)
floats (40%)
150
37
20
15
kDa
MBP
ε-COP
Arf1
MBP-Scyl1
coatomer
myr-Arf1 WT
GTPγS
B
inputs (2%)
floats (40%)
150
75
37
20
15
kDa
MBP
δ-COP
ε-COP
Arf1
MBP-IPIP27A
MBP-Scyl1
coatomer
myr-Arf1 WT
GTPγS
C
MBP-IPIP27A
MBP-Scyl1
% of input in floated fraction
20
15
10
5
0
**
***
Arf1
δ-COP
ε-COP

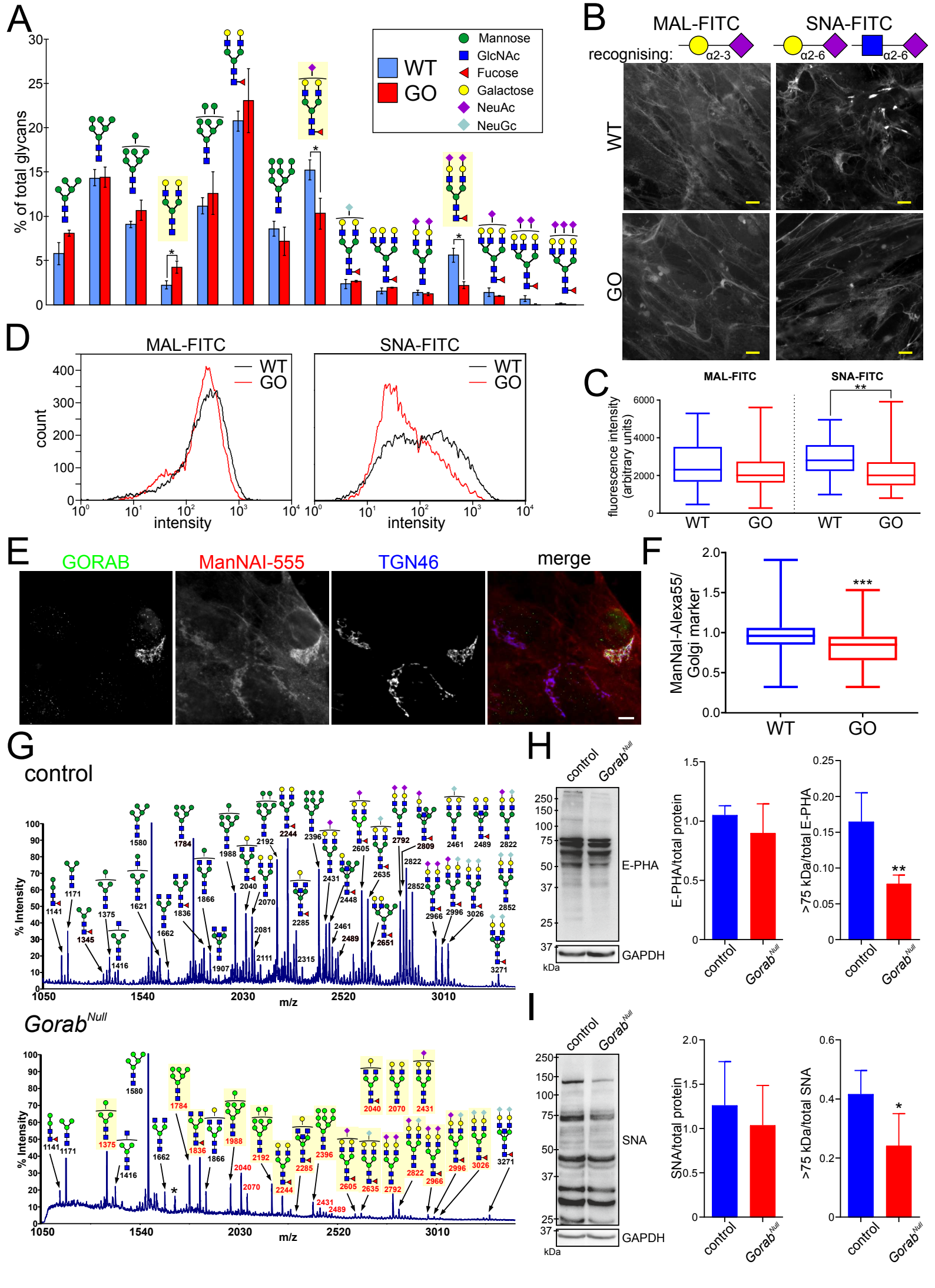
A
% of total glycans
WT
GO
Mannose
GlcNAc
Fucose
Galactose
NeuAc
NeuGc
B
MAL-FITC
SNA-FITC
recognising:
α2-3
α2-6
α2-6
WT
GO
C
MAL-FITC
SNA-FITC
fluorescence intensity (arbitrary units)
WT
GO
WT
GO
D
MAL-FITC
SNA-FITC
count
intensity
intensity
WT
GO
E
GORAB
ManNAl-555
TGN46
merge
F
ManNAl-Alexa55/ Golgi marker
WT
GO
G
control
% Intensity
m/z
Gorab^Null
H
control
Gorab^Null
E-PHA
GAPDH
kDa
E-PHA/total protein
>75 kDa/total E-PHA
I
control
Gorab^Null
SNA
GAPDH
kDa
SNA/total protein
>75 kDa/total SNA

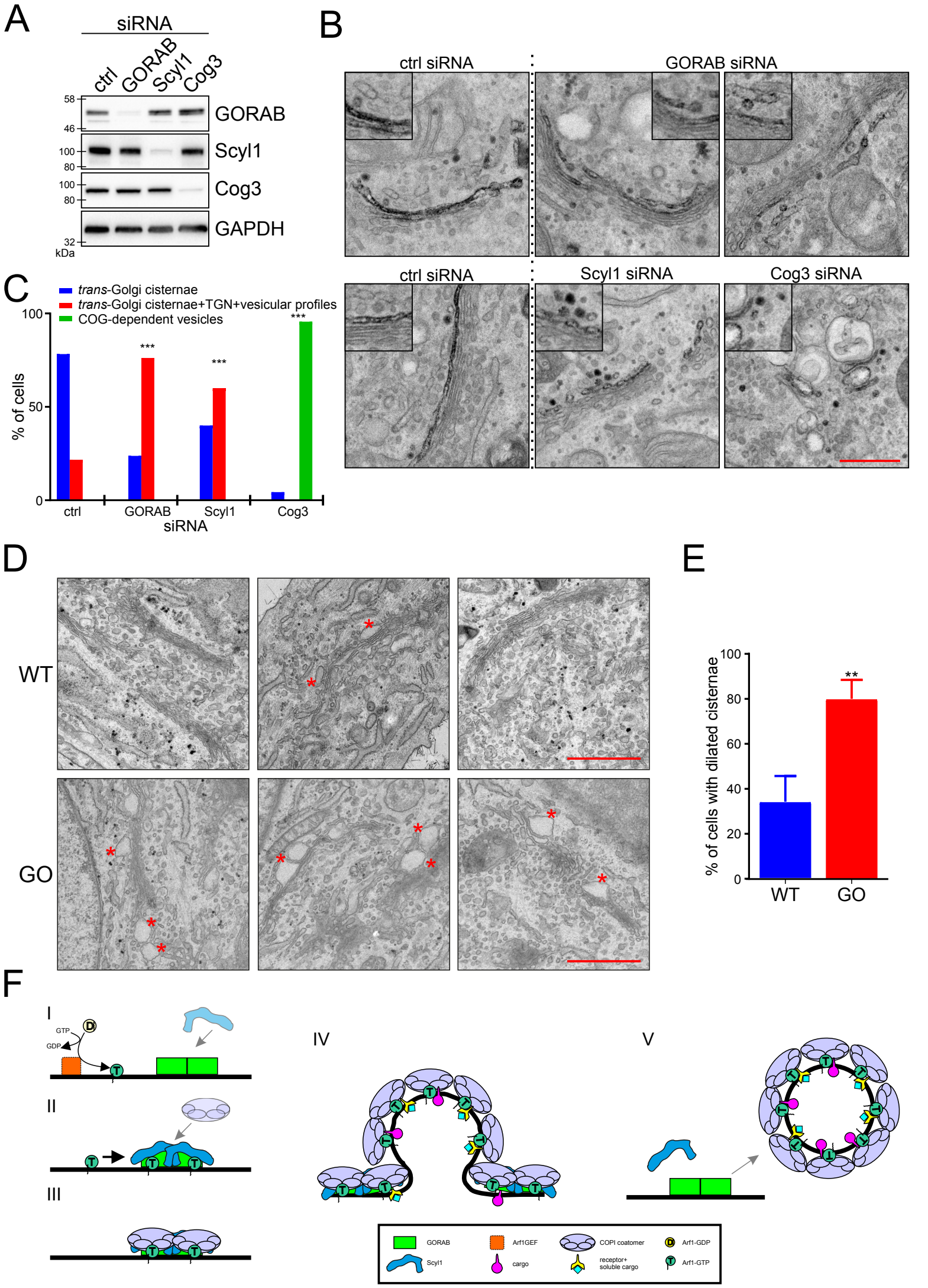
A
siRNA
ctrl
GORAB
Scyl1
Cog3
58
46
100
80
100
80
32
kDa
GORAB
Scyl1
Cog3
GAPDH
B
ctrl siRNA
GORAB siRNA
ctrl siRNA
Scyl1 siRNA
Cog3 siRNA
C
trans-Golgi cisternae
trans-Golgi cisternae+TGN+vesicular profiles
COG-dependent vesicles
100
50
0
% of cells
***
***
***
ctrl
GORAB
Scyl1
Cog3
siRNA
D
WT
GO
E
% of cells with dilated cisternae
100
80
60
40
20
0
**
WT
GO
F
I
GTP
GDP
D
T
II
III
IV
V
GORAB
Scyl1
Arf1GEF
cargo
COPI coatomer
receptor+
soluble cargo
Arf1-GDP
Arf1-GTP